Supplementary Information

A DFT Investigation of Photocatalytic Water Splitting Properties of the InS/GaTe Heterostructure: Direct Z-Scheme vs Traditional Type-II

Redi Kristian Pingak[1,2*], Oliver J. Conquest[1], Catherine Stampfl[1*]

[1]The School of Physics, the University of Sydney, 2006, NSW, Australia

[2]Department of Physics, Faculty of Science and Engineering, University of Nusa Cendana, 85001, Kupang, Indonesia

*Corresponding author: catherine.stampfl@sydney.edu.au; rpin0929@uni.sydney.edu.au
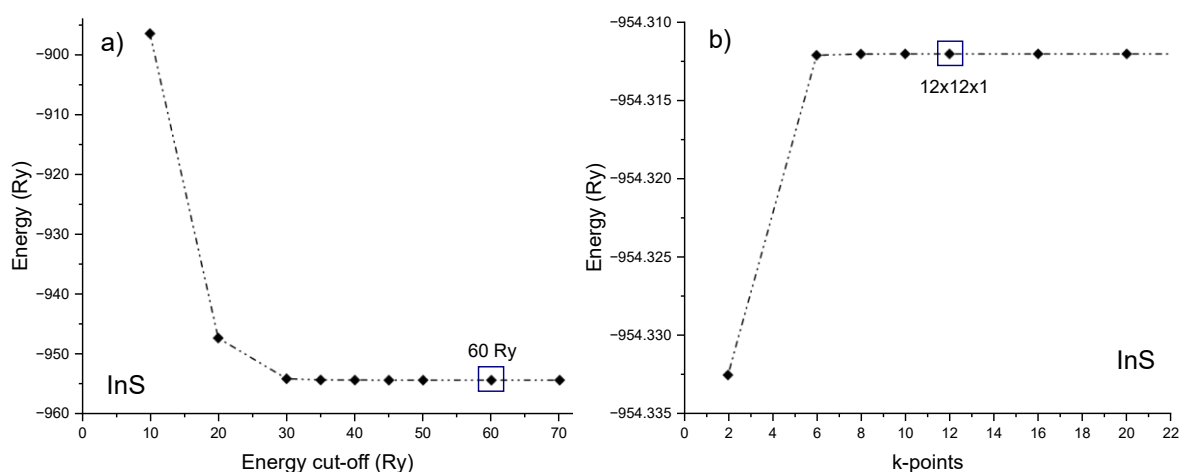
Figure S1. Total energy versus energy cutoff for the InS monolayer (a) and total energy versus k-point mesh (b) where the number "n" represents a "nxnx1" mesh.
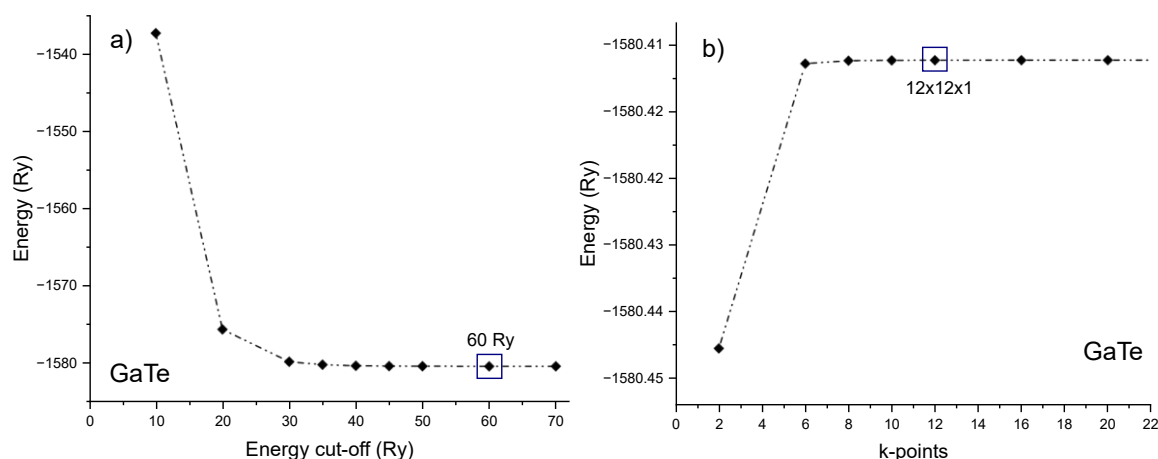

Figure S2. Total energy versus energy cutoff for the GaTe monolayer (a) and total energy versus k-point mesh (b) where the number "n" represents a "nxnx1" mesh.
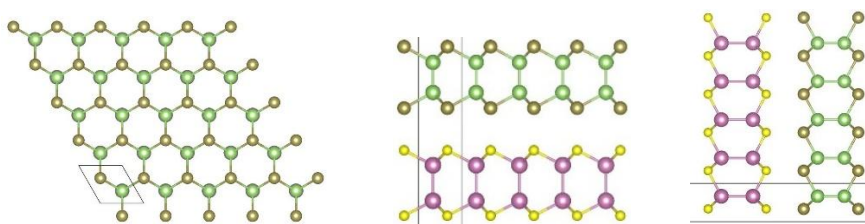
Figure S3. Top and side views of the AA (top) stacking configuration of InS/GaTe. Pink, yellow, green, and brown balls represent In, S, Ga, and Te, respectively.
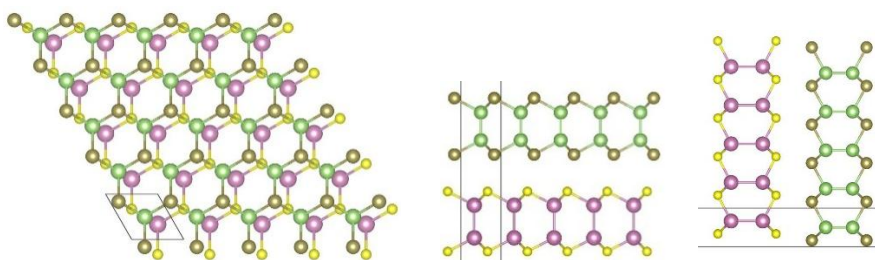

Figure S4. Top and side views of the AB (bridge) stacking configuration of InS/GaTe. Pink, yellow, green, and brown balls represent In, S, Ga, and Te, respectively.
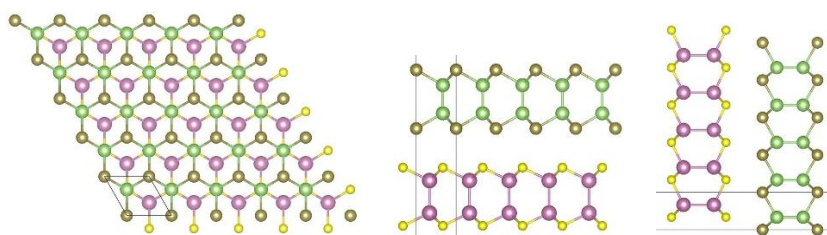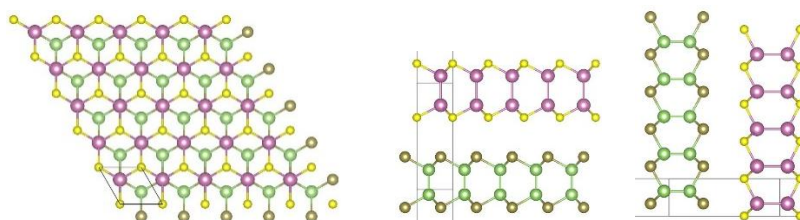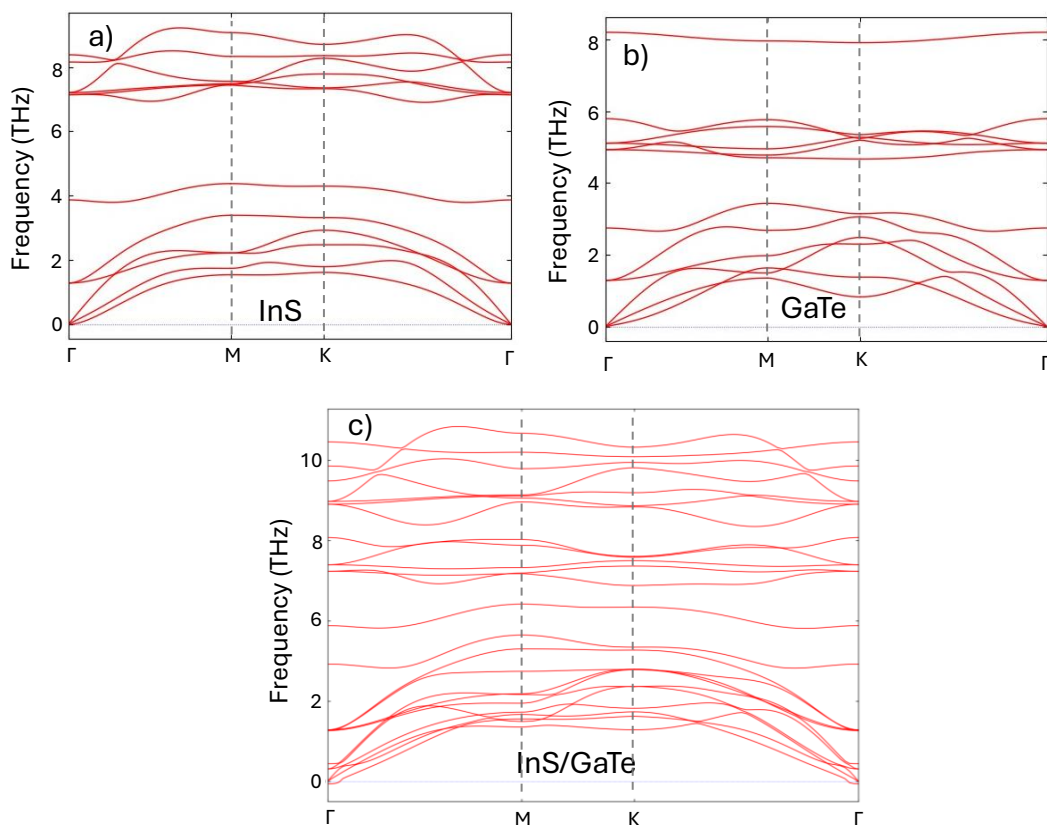

Figure S5. Top and side views of the AC1 (hollow1) stacking configuration of InS/GaTe. Pink, yellow, green, and brown balls represent In, S, Ga, and Te, respectively.

Figure S6. Top and side views of the AC2 (hollow2) stacking configuration of InS/GaTe. Pink, yellow, green, and brown balls represent In, S, Ga, and Te, respectively.

Figure S7. Phonon dispersion curves for the InS (a) and GaTe (b) monolayers, and the InS/GaTe heterostructure (c).
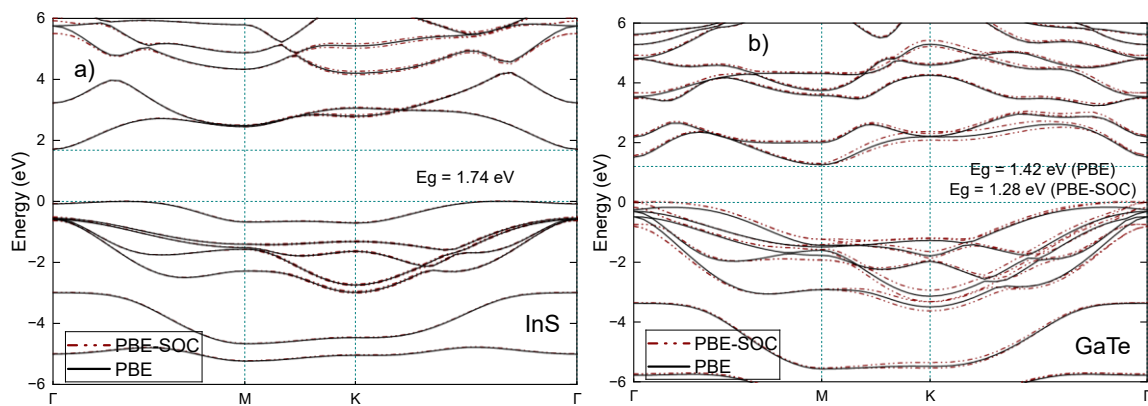
Figure S8. The electronic band structure of InS (a) and GaTe (b) monolayers obtained using PBE and PBE+SOC.
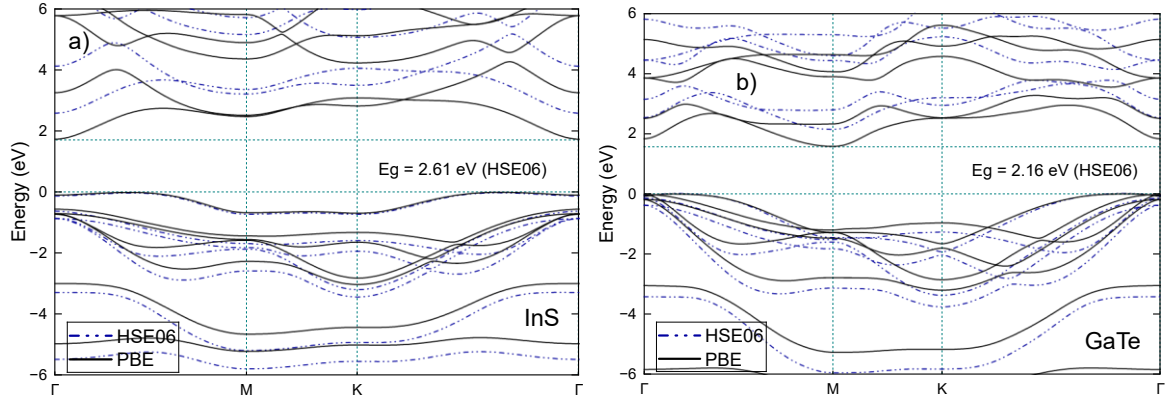
Figure S9. The electronic band structure of InS (a) and GaTe (b) monolayers as obtained using the HSE06 functional.
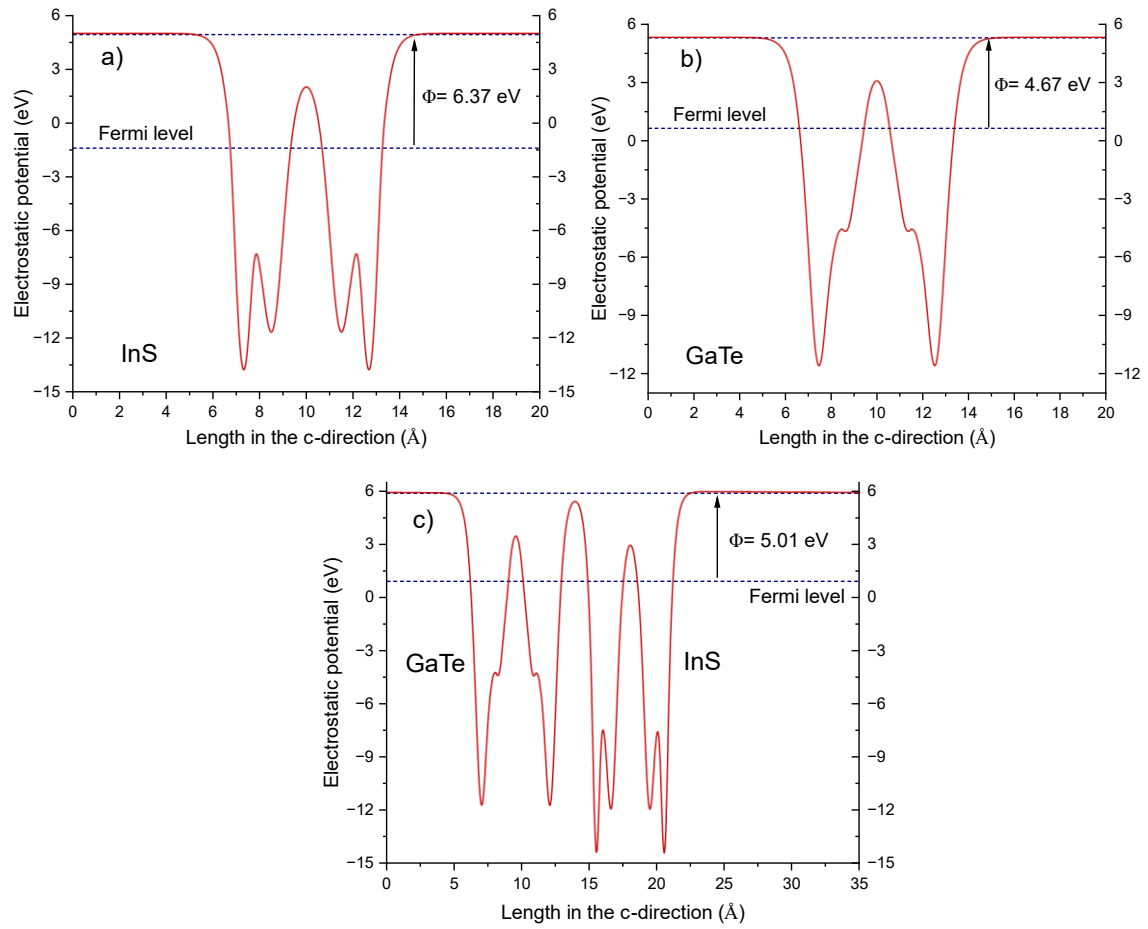
Figure S10. The xy-averaged electrostatic potential of InS (a), GaTe (b), and of the InS/GaTe heterostructure (c) as obtained using the HSE06 functional.
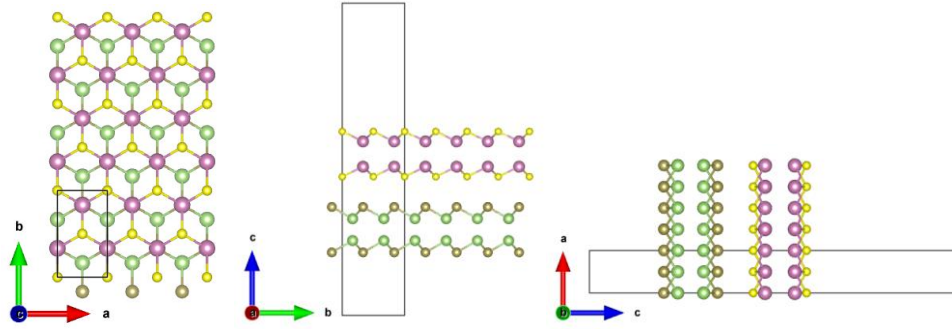
Figure S11. The rectangular unit cell: the x (zig-zag, along **a**) and y (arm-chair, along **b**) directions are represented by a and b axes, respectively. Pink, yellow, green, and brown balls represent In, S, Ga, and Te, respectively.
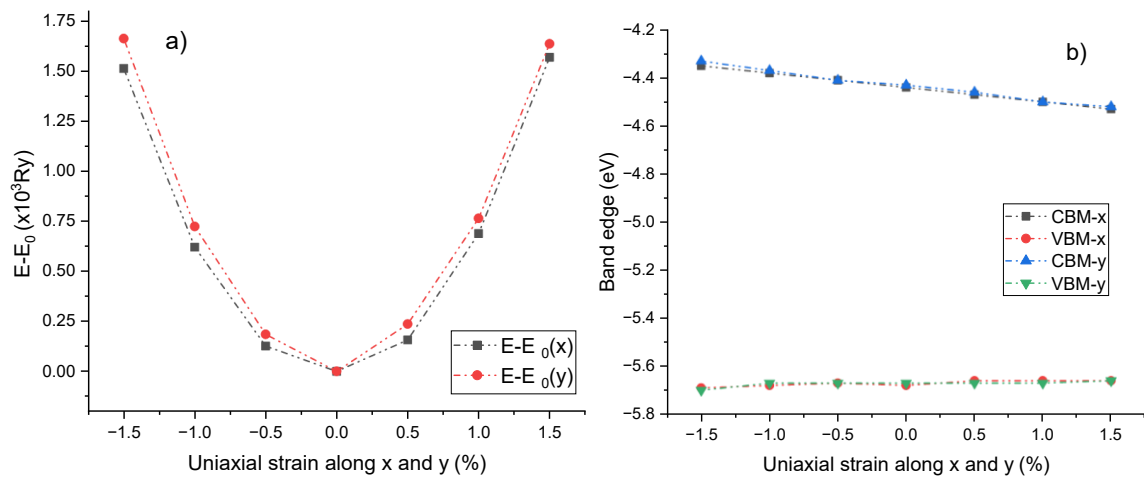
Figure S12. The relative energy (a) and the variation in the band edges (b) of the InS/GaTe heterostructure versus the uniaxial strain along x and y directions.
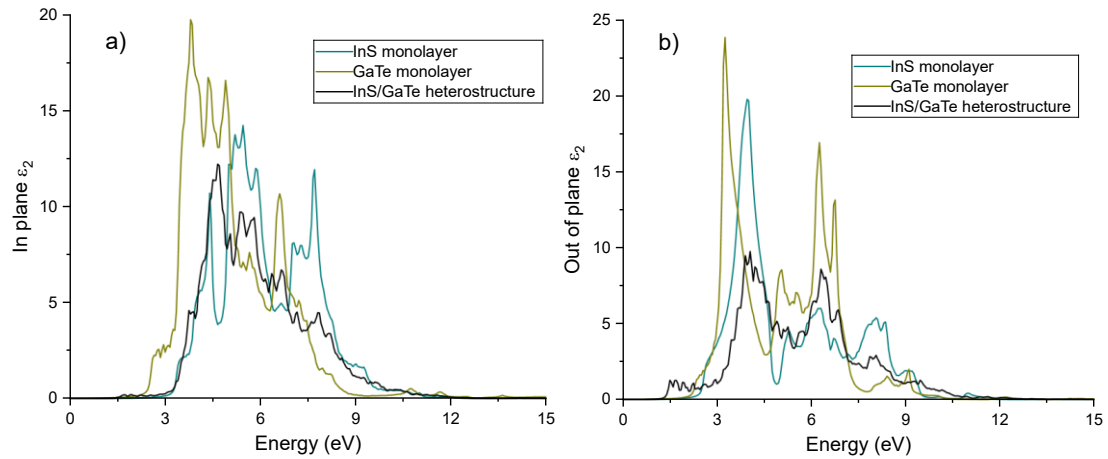
Figure S13. Imaginary part of the dielectric function of the InS and GaTe monolayers as well as the InS/GaTe heterostructure, obtained using the HSE06 functional: in plane (a) and out of plane (b).
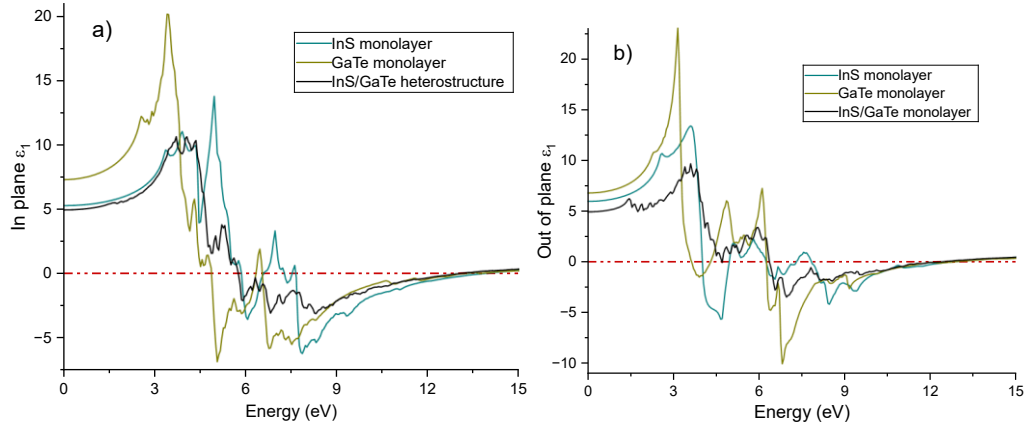
Figure S14. Real part of the dielectric function of the InS and GaTe monolayers as well as the InS/GaTe heterostructure, calculated using the HSE06 functional: in plane (a) and out of plane (b).
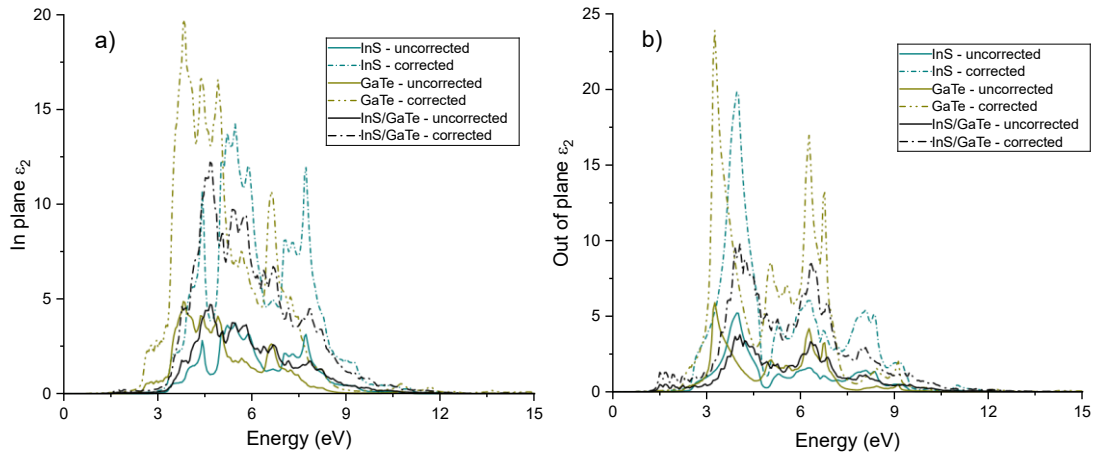
Figure S15. Imaginary part of the dielectric function of the InS and GaTe monolayers as well as the InS/GaTe heterostructure, obtained using the HSE06 functional, for in-plane (a) and out-of-plane (b). "Uncorrected" means the calculated values still include the vacuum effect while "corrected" means that the vacuum effect has been renormalized using the method presented in Ref [1].
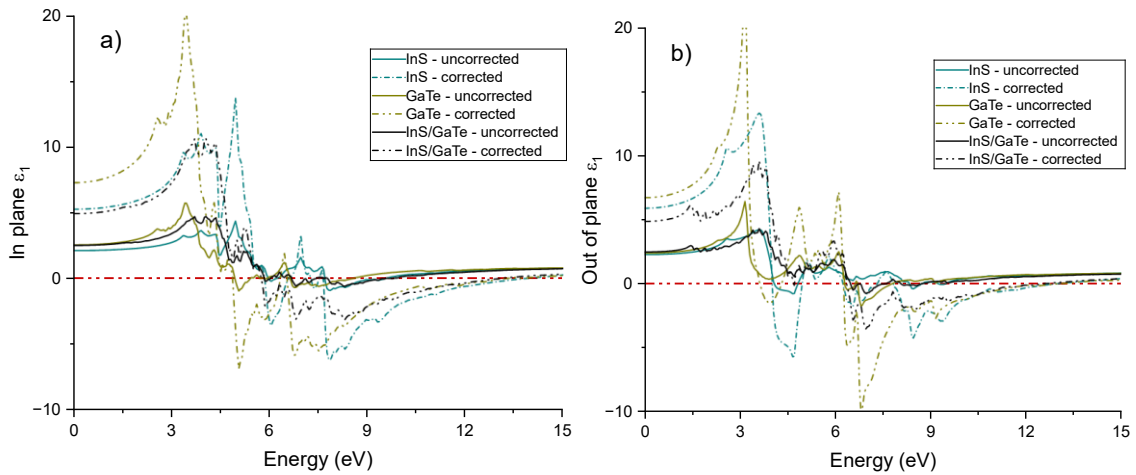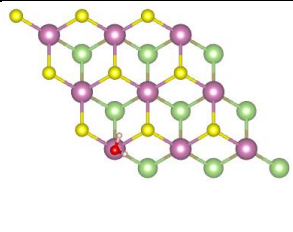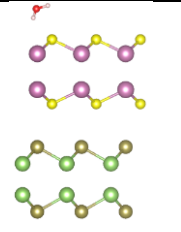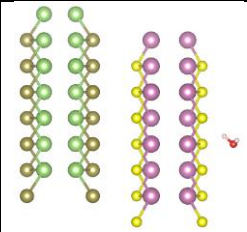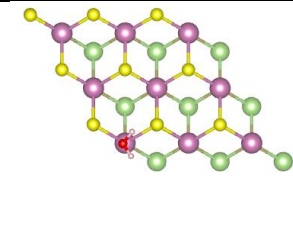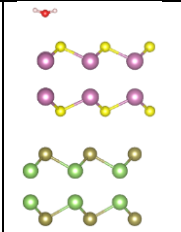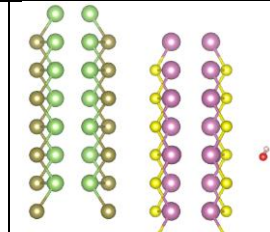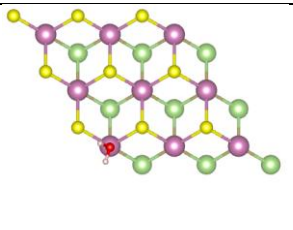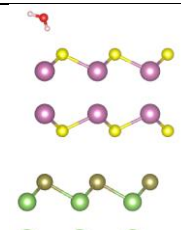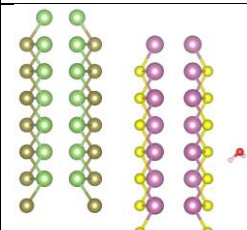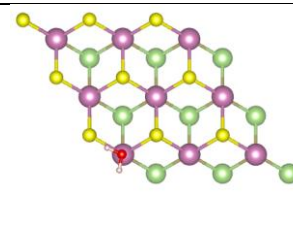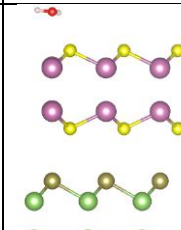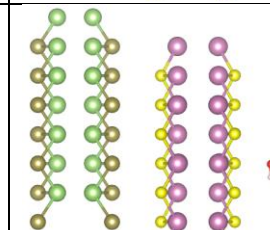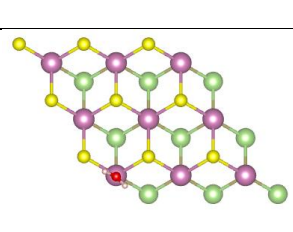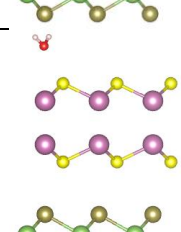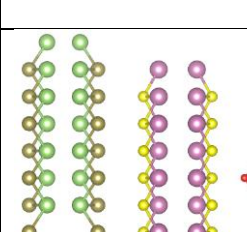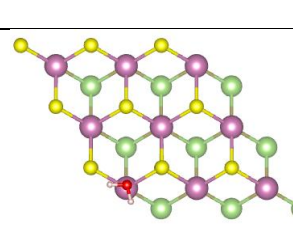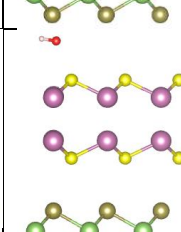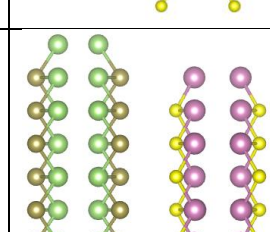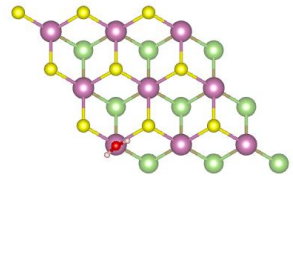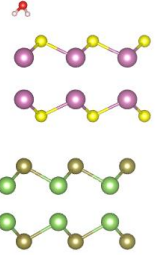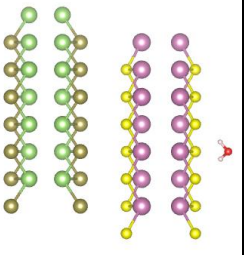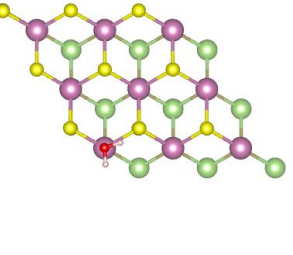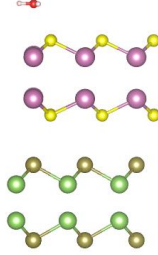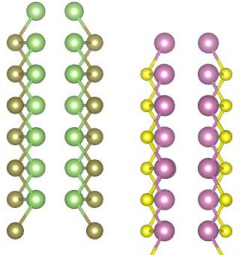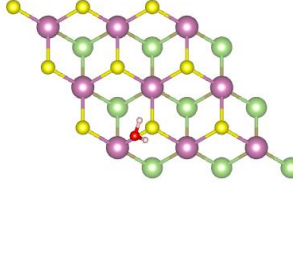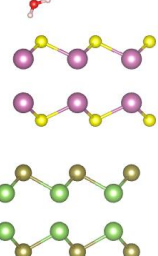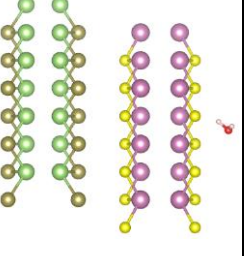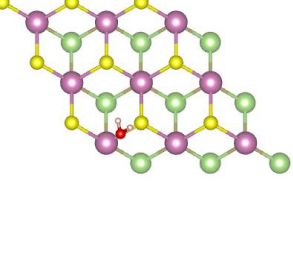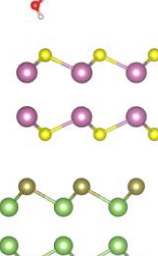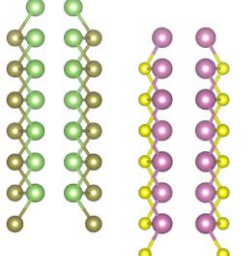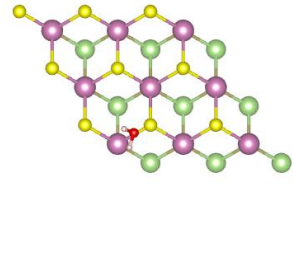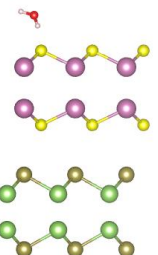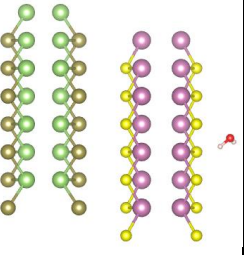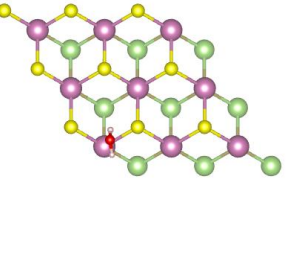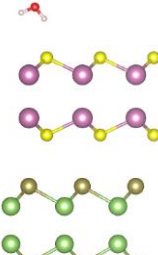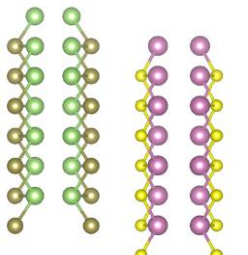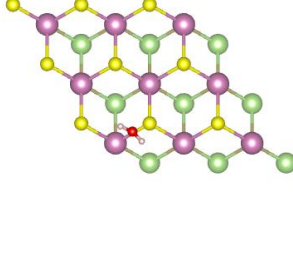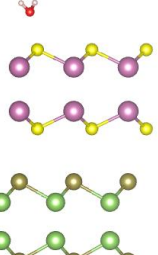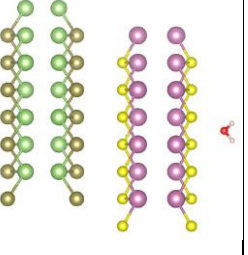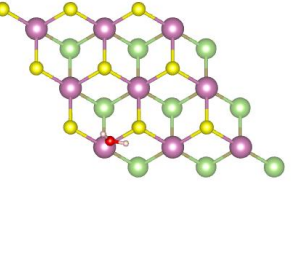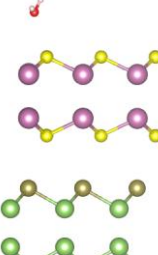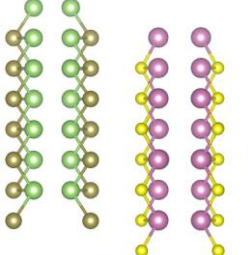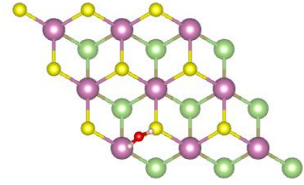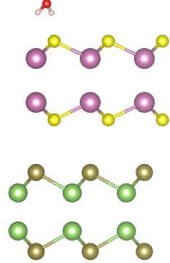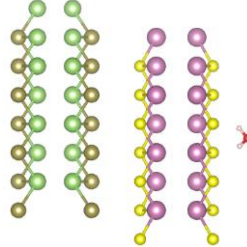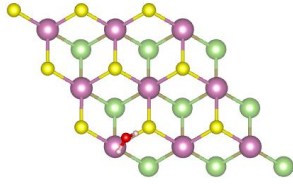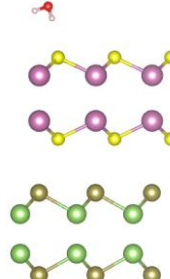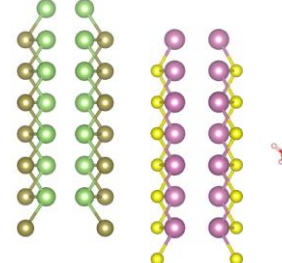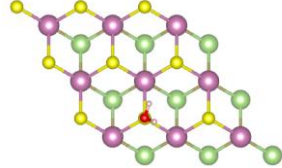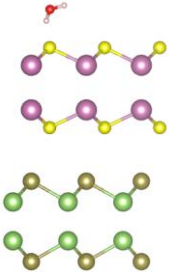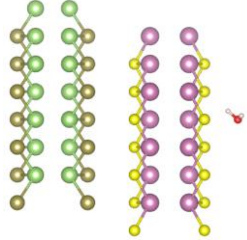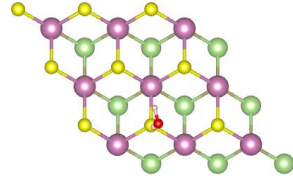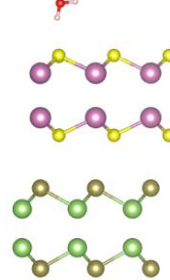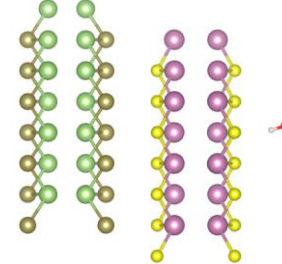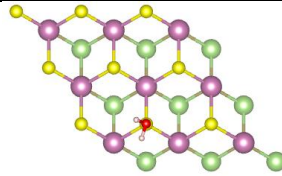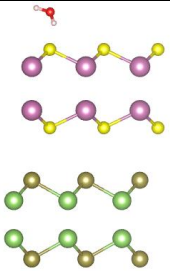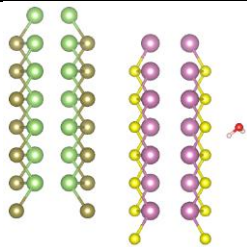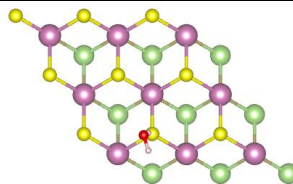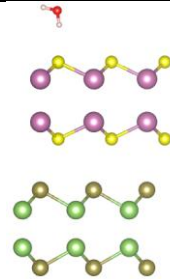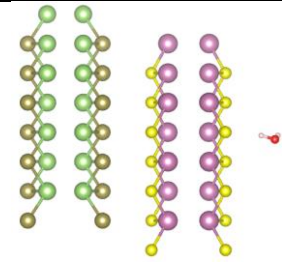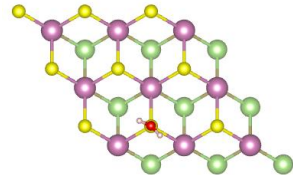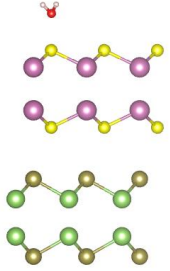
Figure S16. Real part of the dielectric function of the InS and GaTe monolayers as well as the InS/GaTe heterostructure calculated using the HSE06 functional, for in-plane (a) and out-of-plane (b). "Uncorrected" means the calculated values still include the vacuum effect while "corrected" means that the vacuum effect has been renormalized using the method presented in Ref [1].
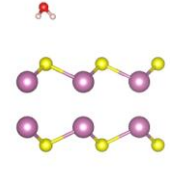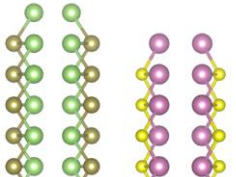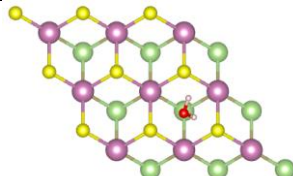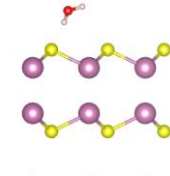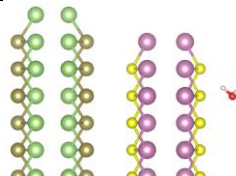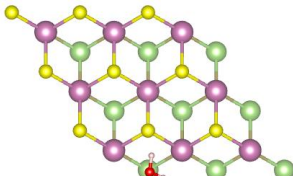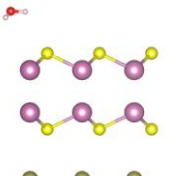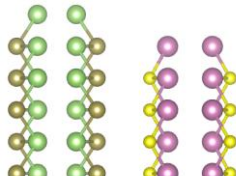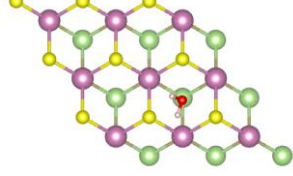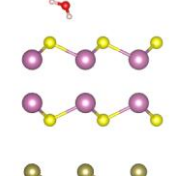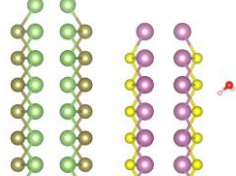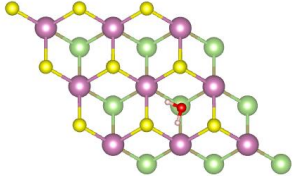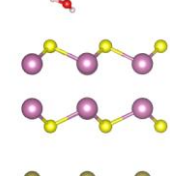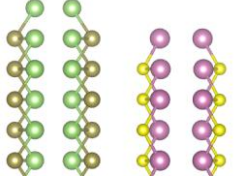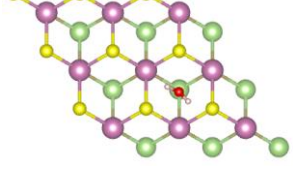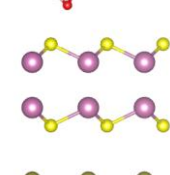
Table S1. H_2O adsorption on the InS surface.
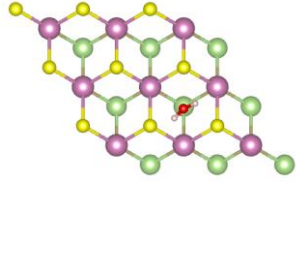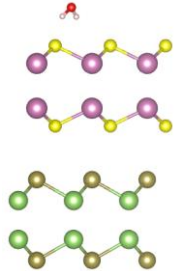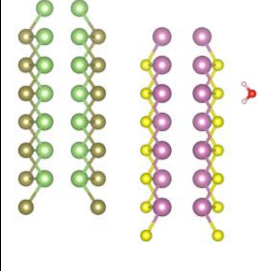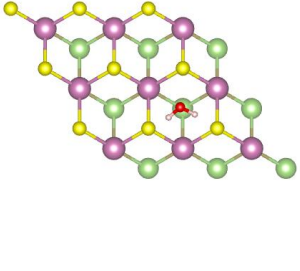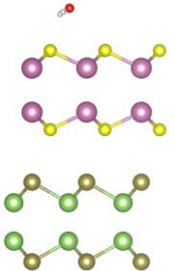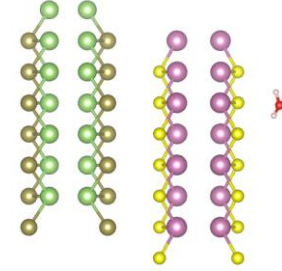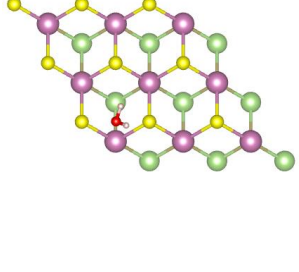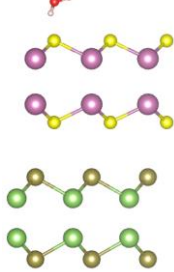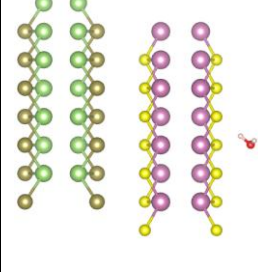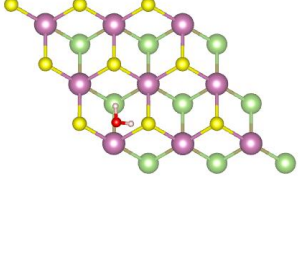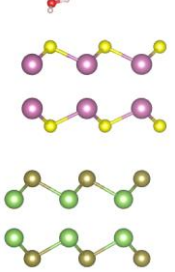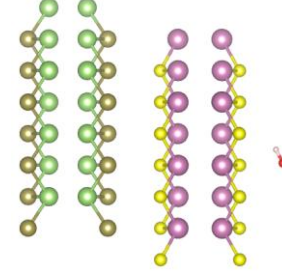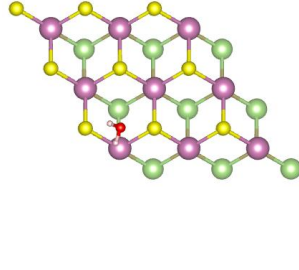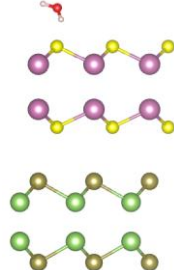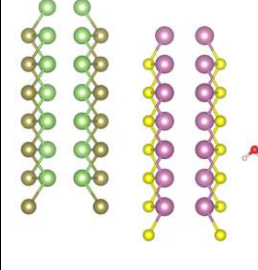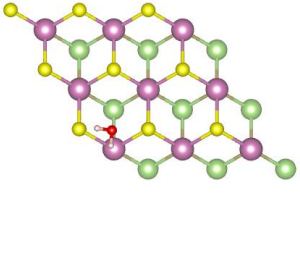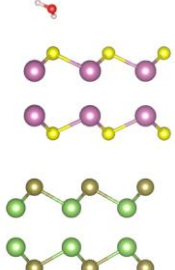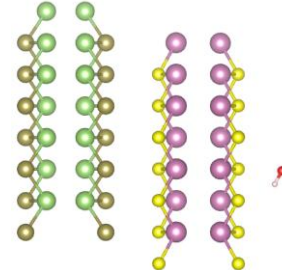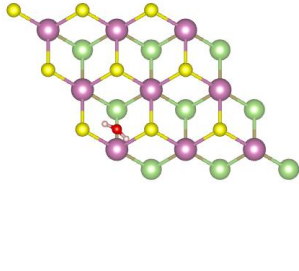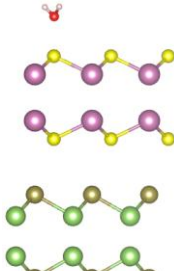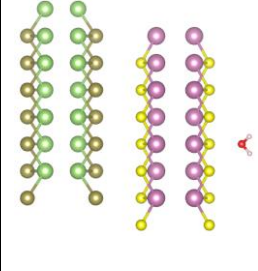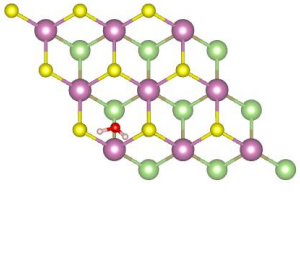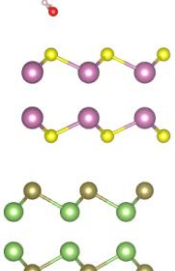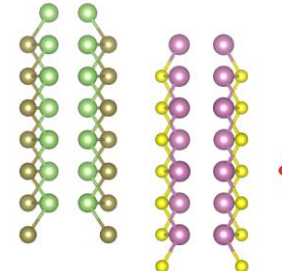
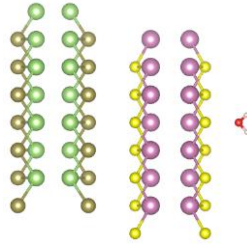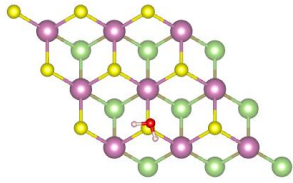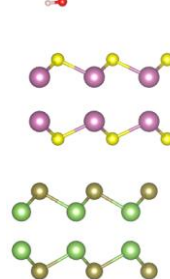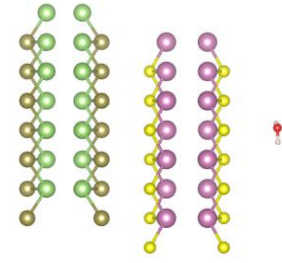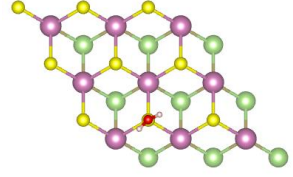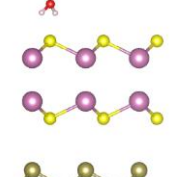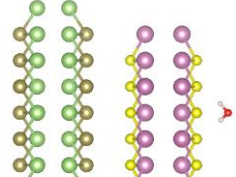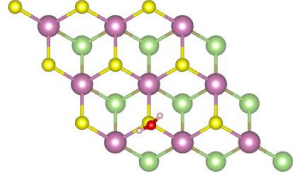There are 6 different H_2O adsorption sites considered, each with 4 different rotation angles of H_2O. The optimized structures with the corresponding adsorption energy are presented in the following table, along with the initial configurations. The most favourable configuration is the configuration number 4 (highlighted in green) with adsorption energy of -0.194 eV.
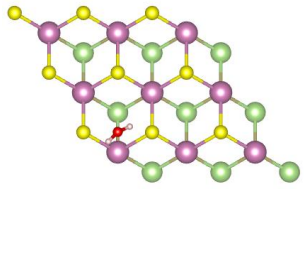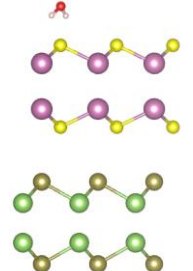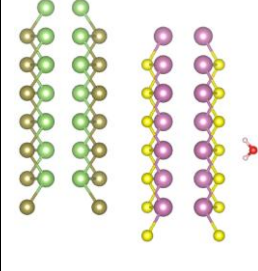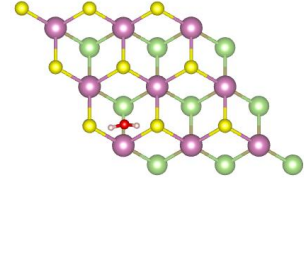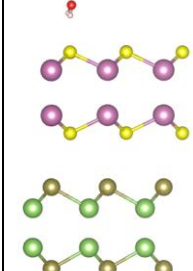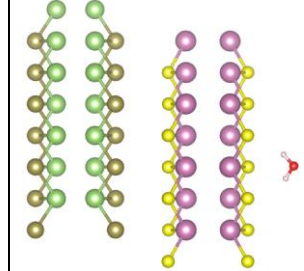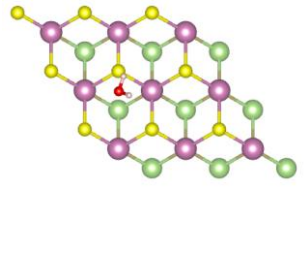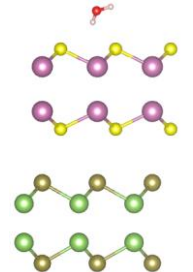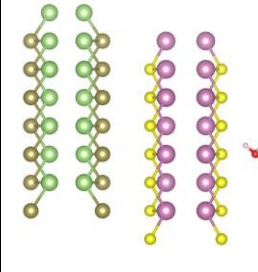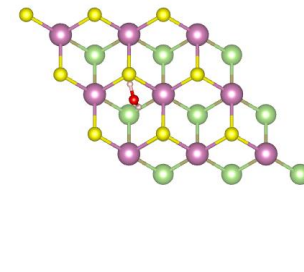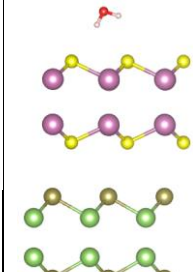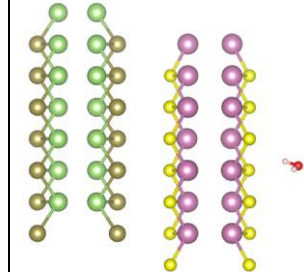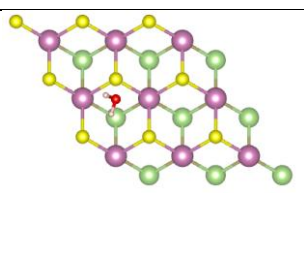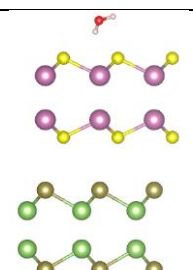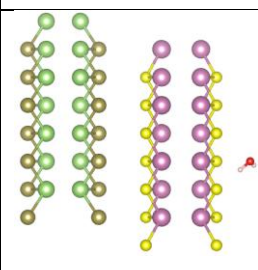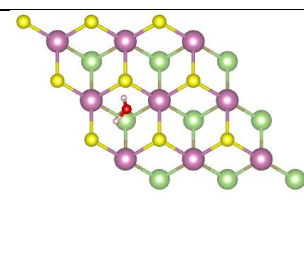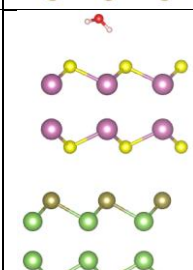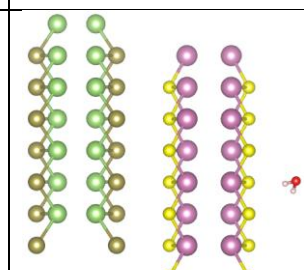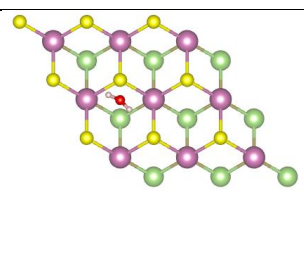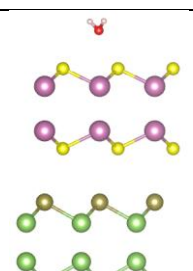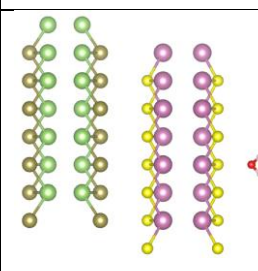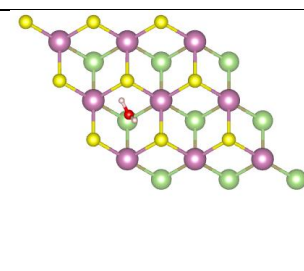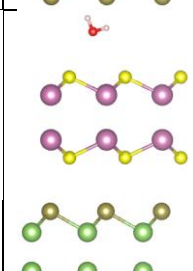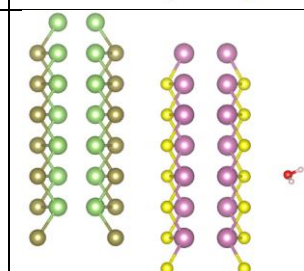
No	Initial			Optimized			E_ads (eV)
	Top	Side-1	Side-2	Top	Side-1	Side-2	
1							-0.166
2							-0.189
3							-0.175

4							-0.194
5							-0.138
6							-0.108
7							-0.122

8						-0.141
9						-0.122
10						-0.125
11						-0.055

12						-0.089
13						-0.168
14						-0.132
15						-0.150

16		-0.170
17		-0.148
18		-0.149
19		-0.134

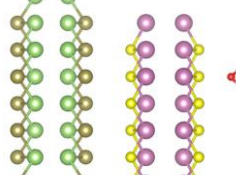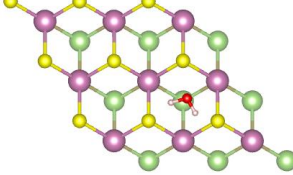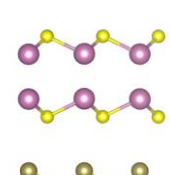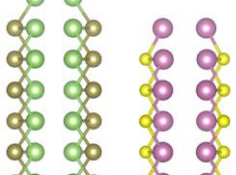| 20							-0.164
21							-0.126
22							-0.154
23							-0.117
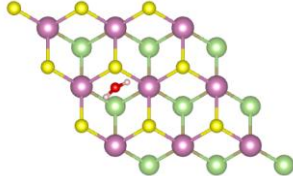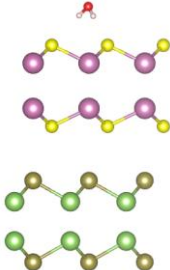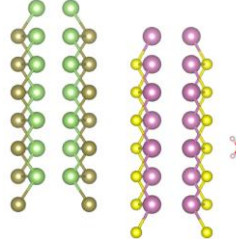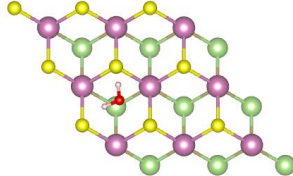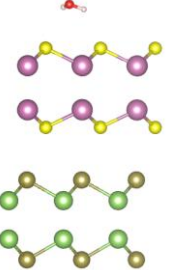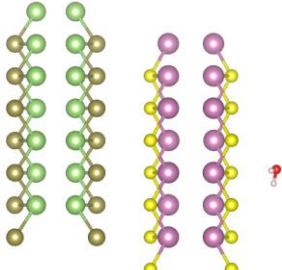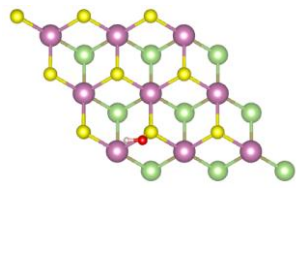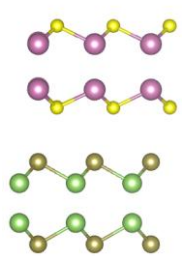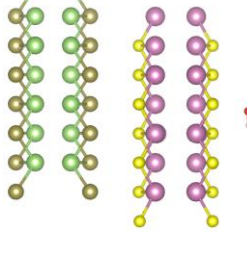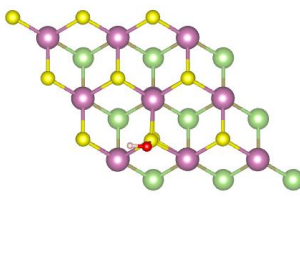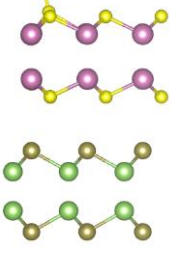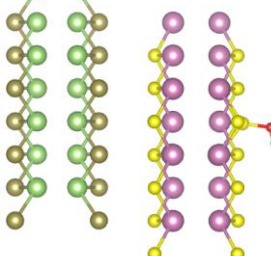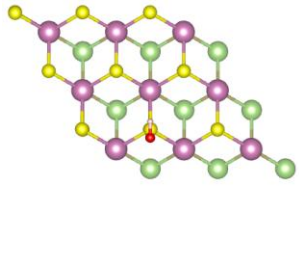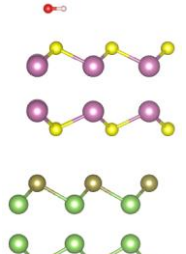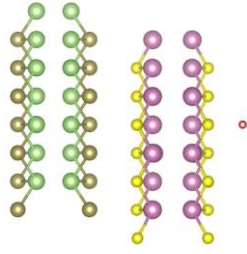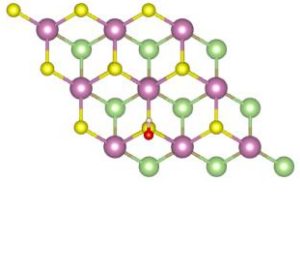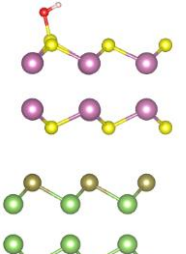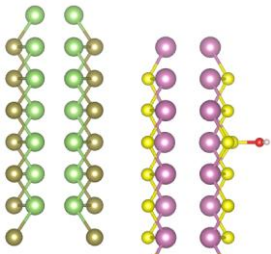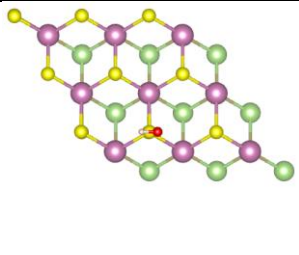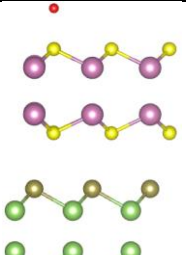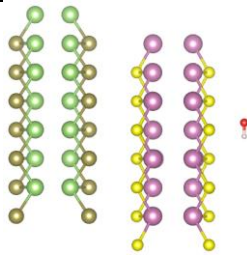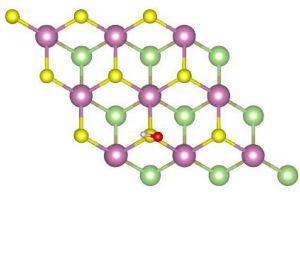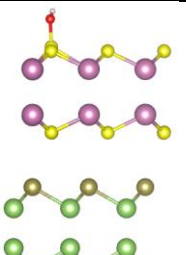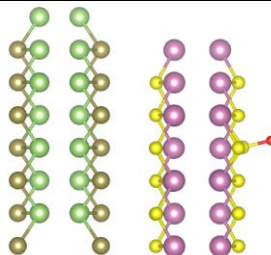
| 24 | | -0.159 |

Table S2. OH adsorption on the InS surface.

24 different configurations were studied, from which 7 stable adsorption sites obtained. The optimized structures with the corresponding adsorption energy are presented in the following table, along with the initial configurations. Configuration number 1 (highlighted in green) is the most favourable one with adsorption energy of -1.383 eV.

No	Initial			Optimized			E_ads (eV)
	Top	Side-1	Side-2	Top	Side-1	Side-2	
1							-1.383
2							-1.355
3							-1.358
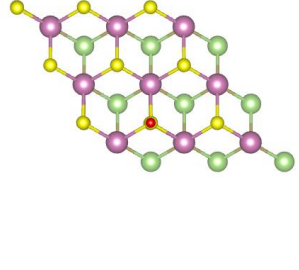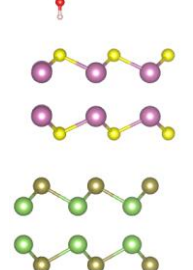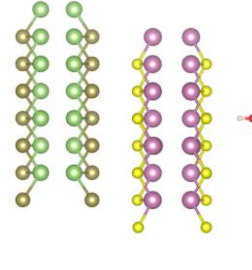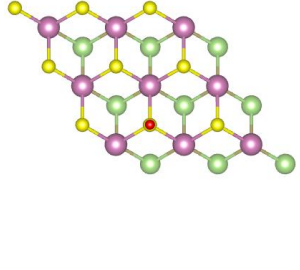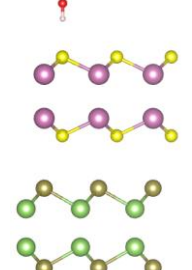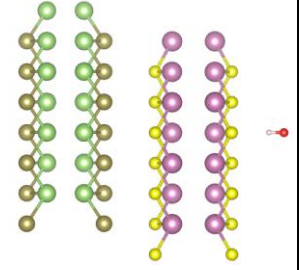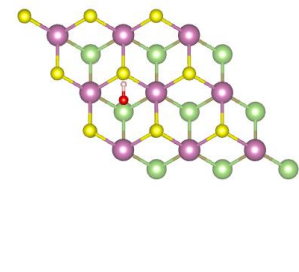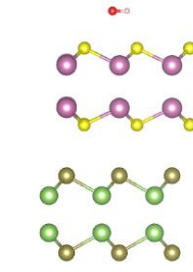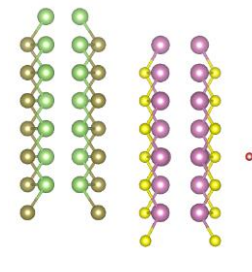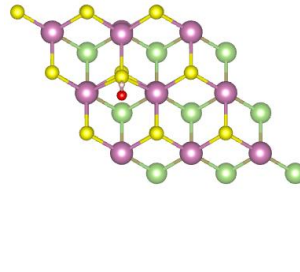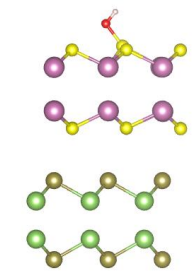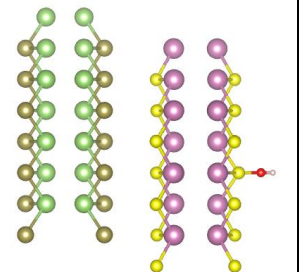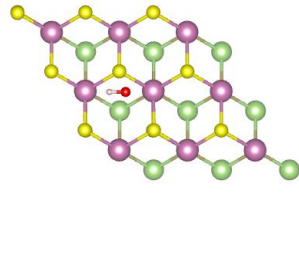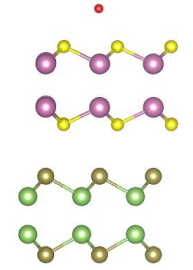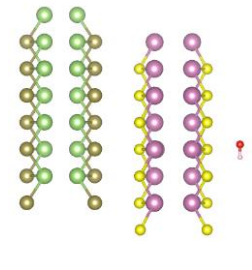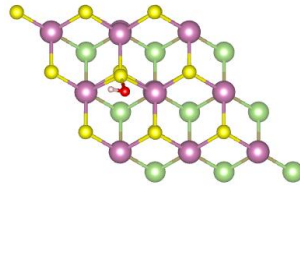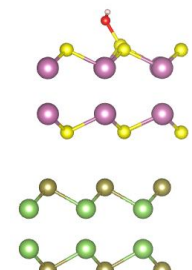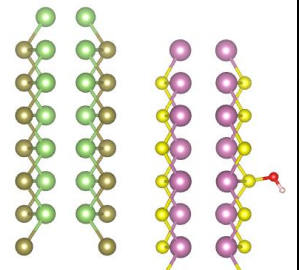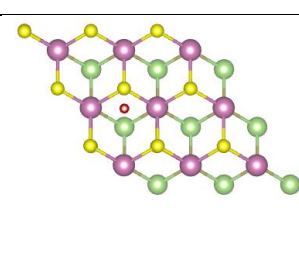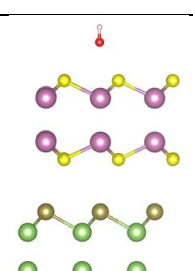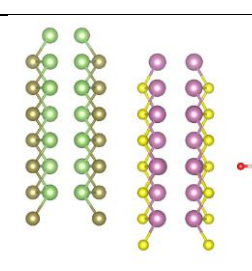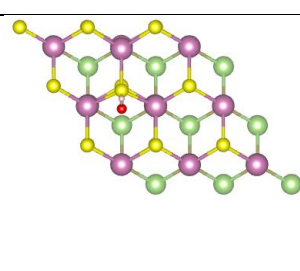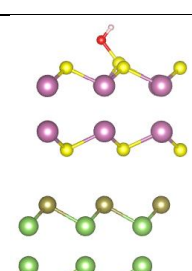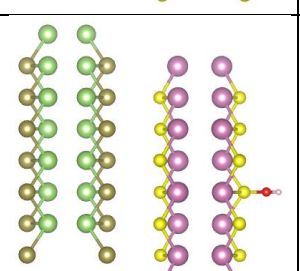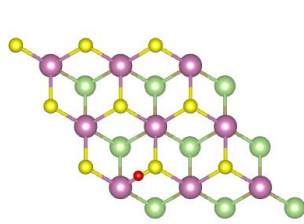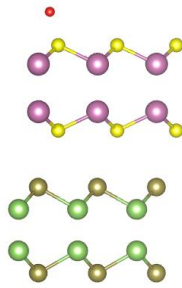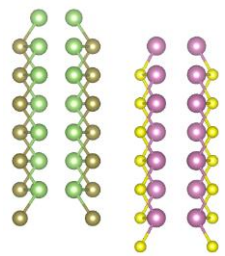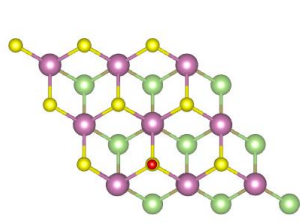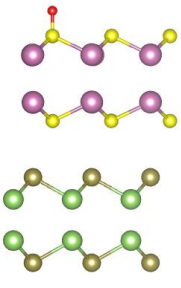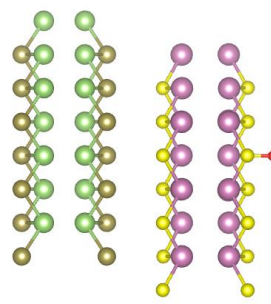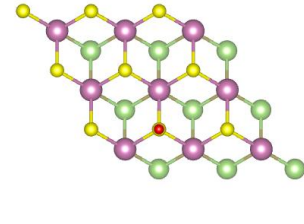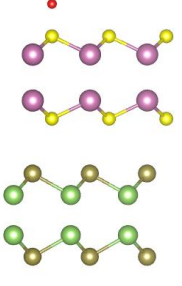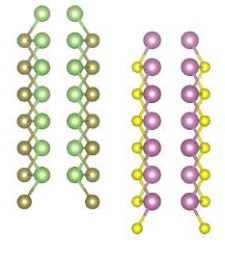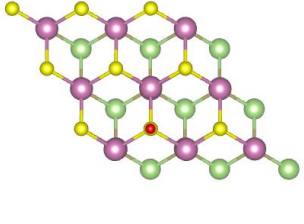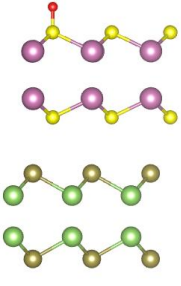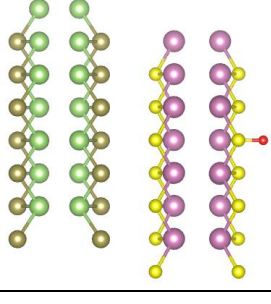
4							-0.299
5							-0.126
6							-0.154
7							-0.117

Table S3. O adsorption on the InS surface.

6 different configurations were studied, from which O was stably adsorbed in 3 configurations. The optimized structures with the corresponding adsorption energy are presented in the following table, along with the initial configurations. Configuration number 3 (highlighted in green) is the most favourable one with adsorption energy of -4.6 eV. It is interesting to note that all the optimized structures imply that the only site for the adsorption of O is on the top of S, with essentially the same adsorption energy of around -4.6 eV.

No	Initial			Optimized			E_ads (eV)
	Top	Side-1	Side-2	Top	Side-1	Side-2	
1							-4.599
2							-4.595

| 3 | | | | | | | -4.600 |
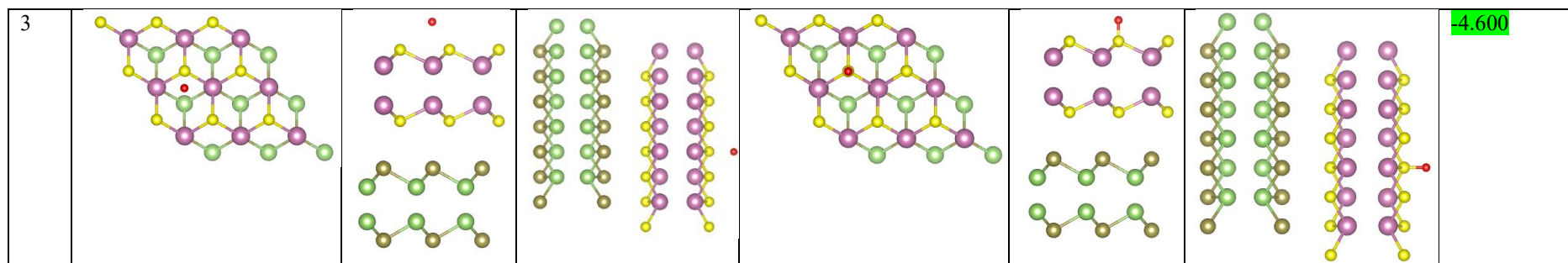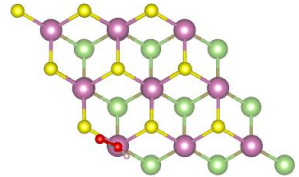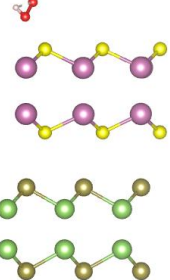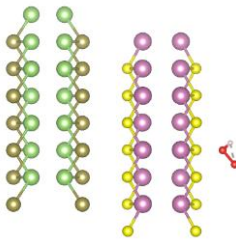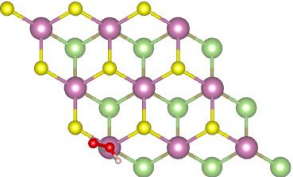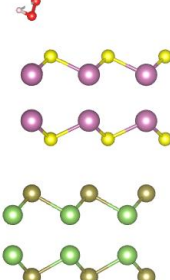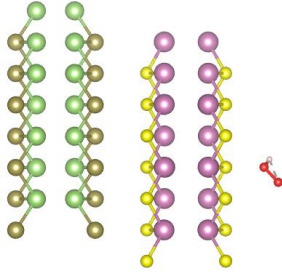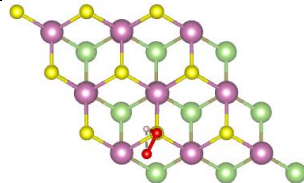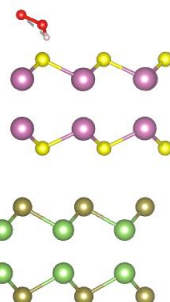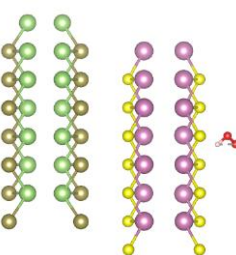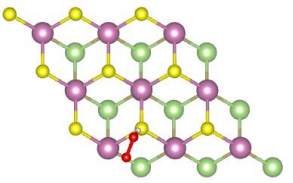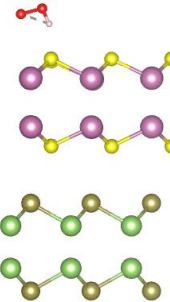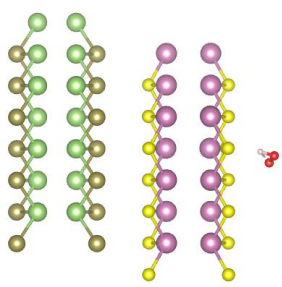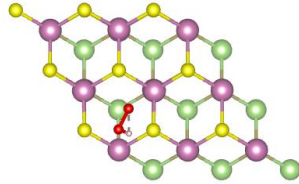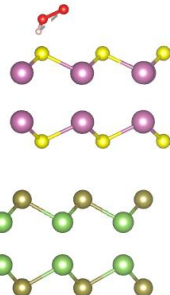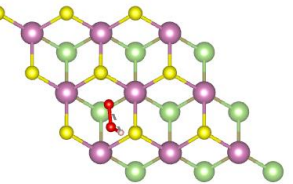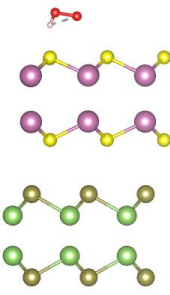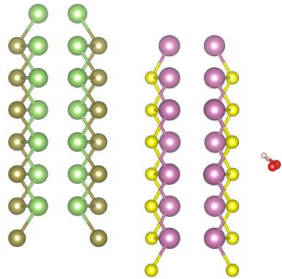
Table S4. OOH adsorption on the InS surface.

24 different configurations were studied, which resulted in 6 stable configurations. The optimized structures with the corresponding adsorption energy are presented in the following table, along with the initial configurations. The configuration number 5 (highlighted in green) is the most favourable one with adsorption energy of -0.331 eV.

No	Initial			Optimized			E_ads (eV)
	Top	Side-1	Side-2	Top	Side-1	Side-2	
1							-0.145
2							-0.321
3							-0.299
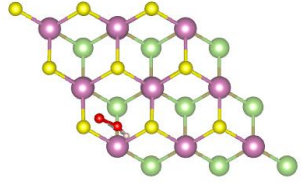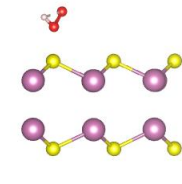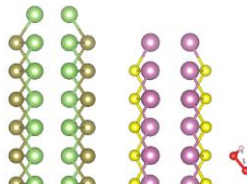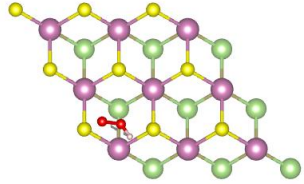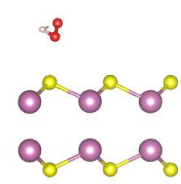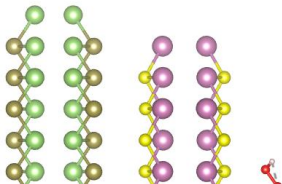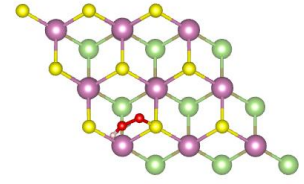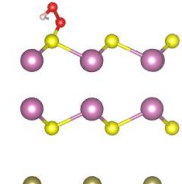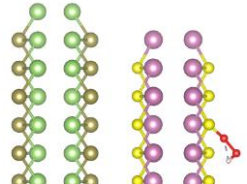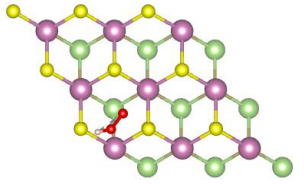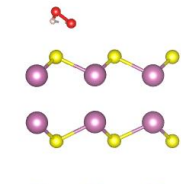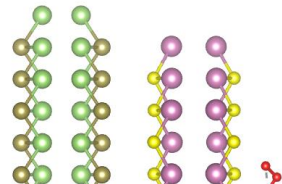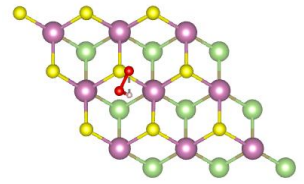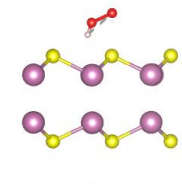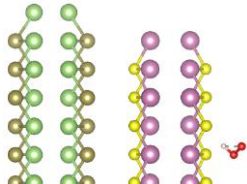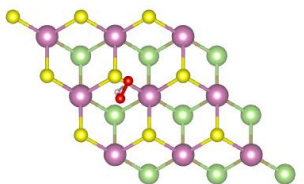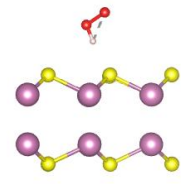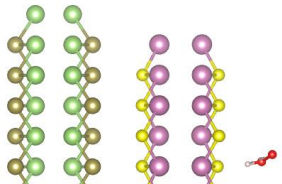
4							-0.124
5							-0.331
6							-0.244

Table S5. H adsorption on the GaTe surface.

6 possible configurations were investigated which resulted in two stable configurations. The optimized structures with the corresponding adsorption energy are presented in the following table, along with the initial configurations. Configuration 1 (highlighted in green) is the most favourable configuration with adsorption energy of -1.926 eV. The adsorption energy was calculated using the energy of the free H atom.
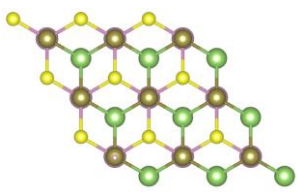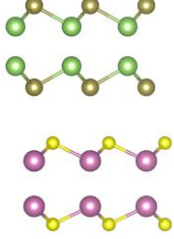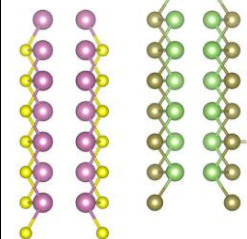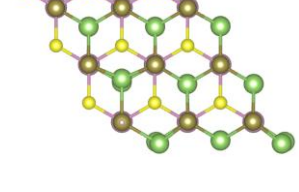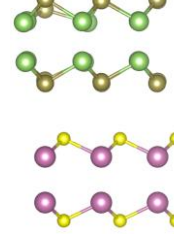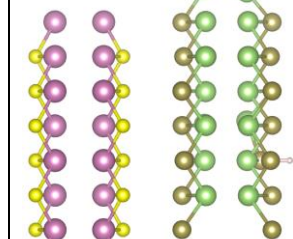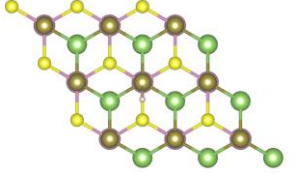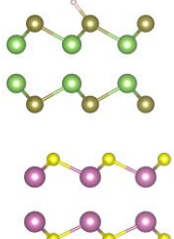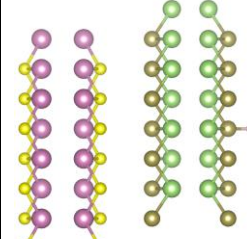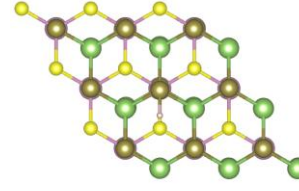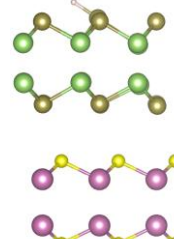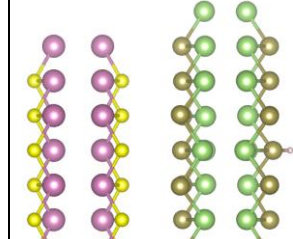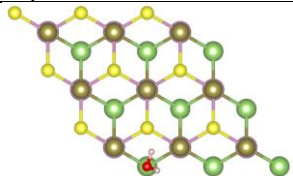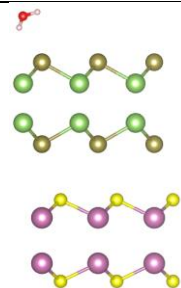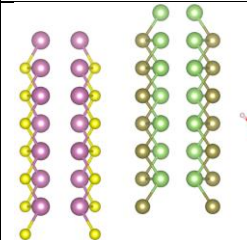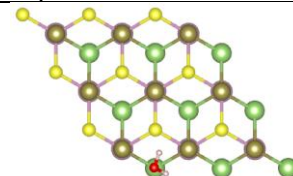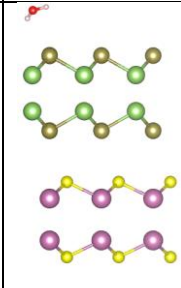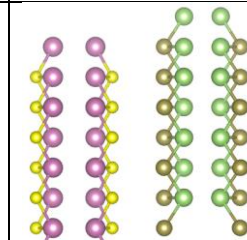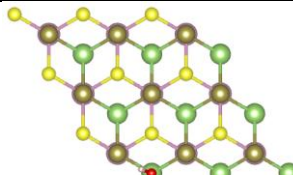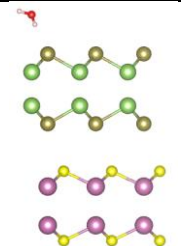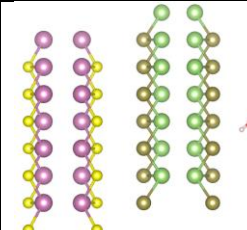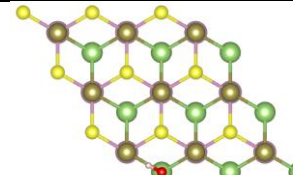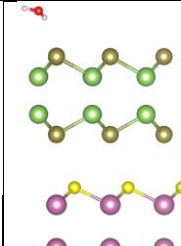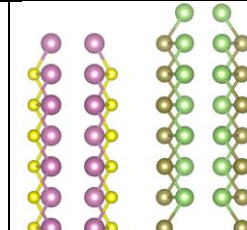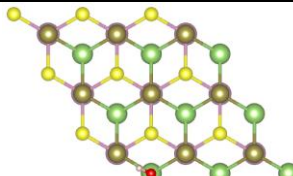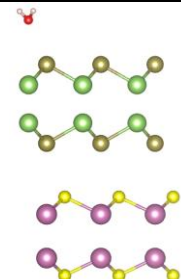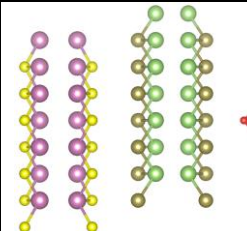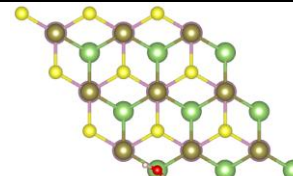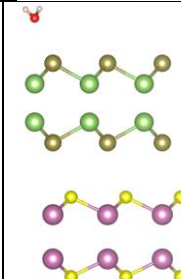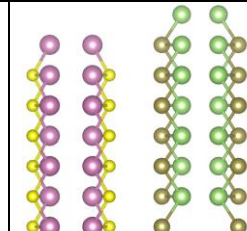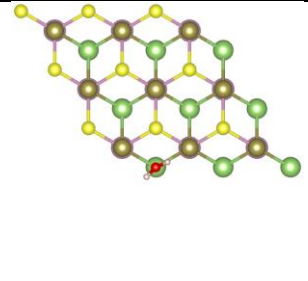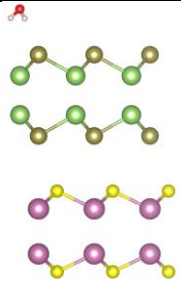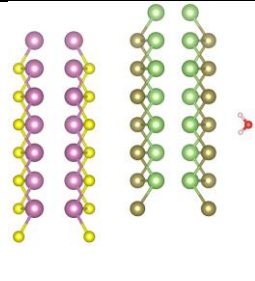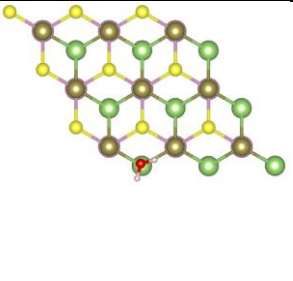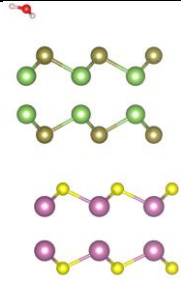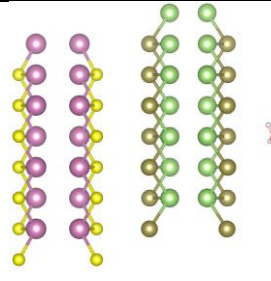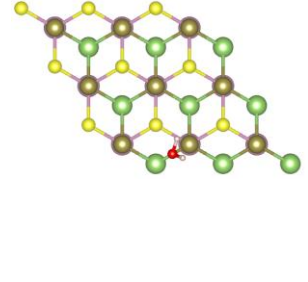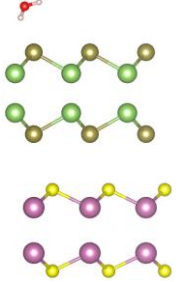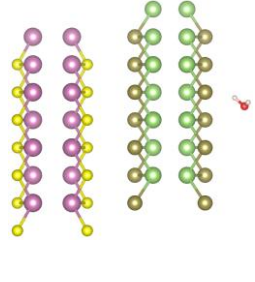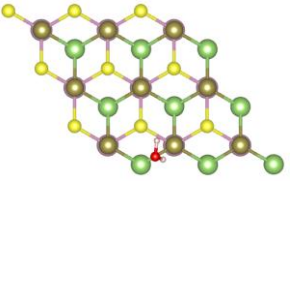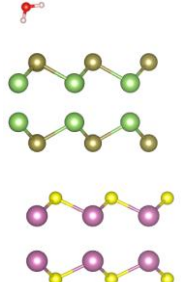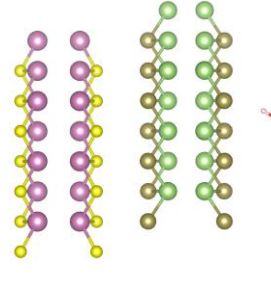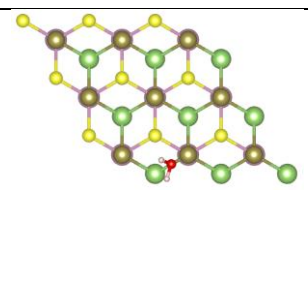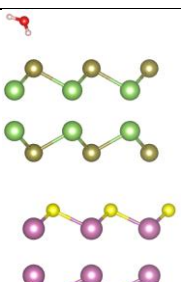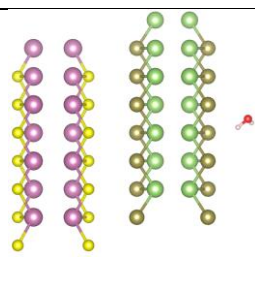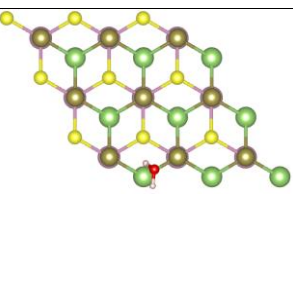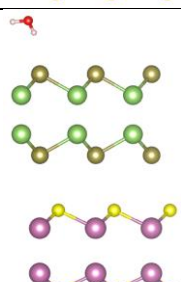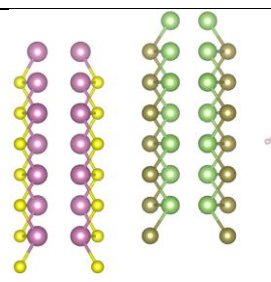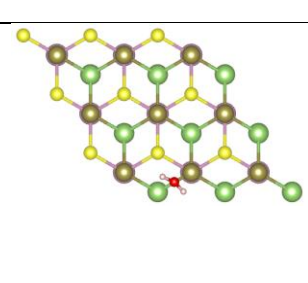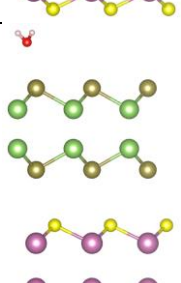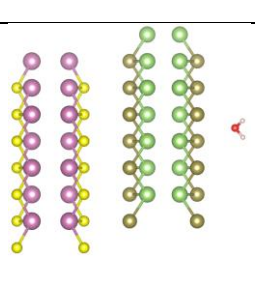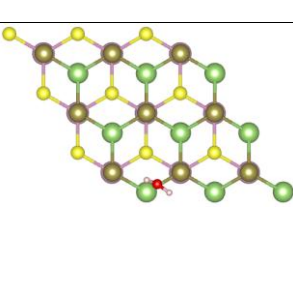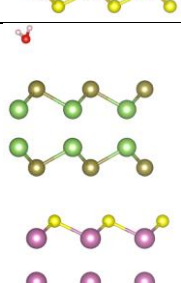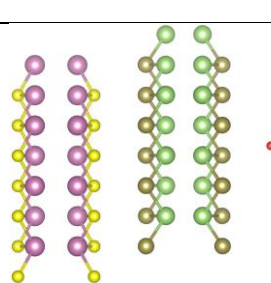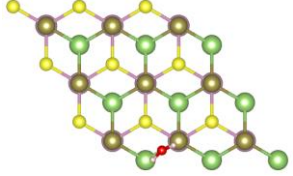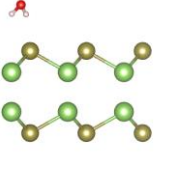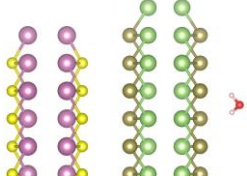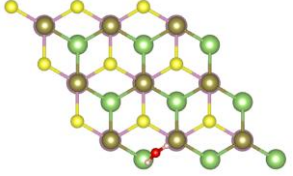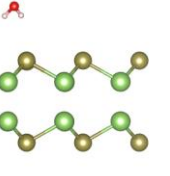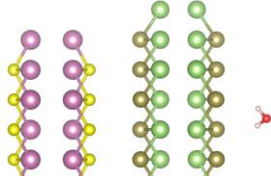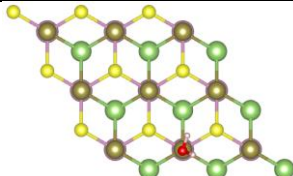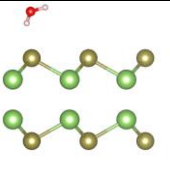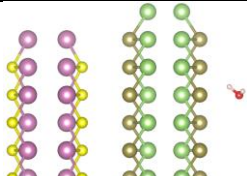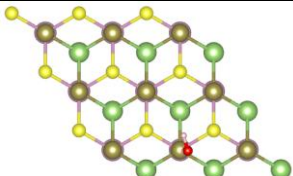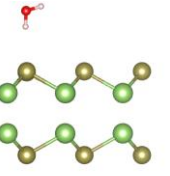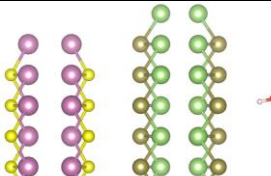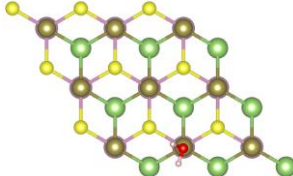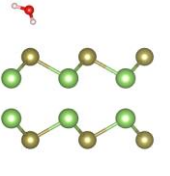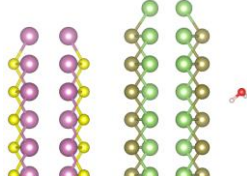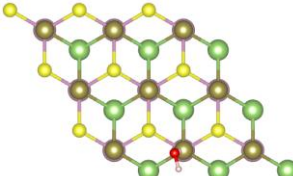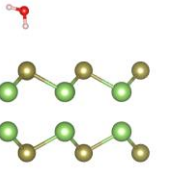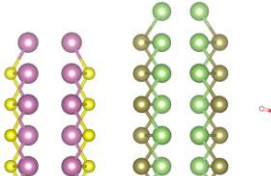
No	Initial			Optimized			E_ads (eV)
	Top	Side-1	Side-2	Top	Side-1	Side-2	
1							-1.926
2							-1.776
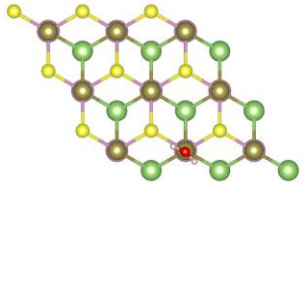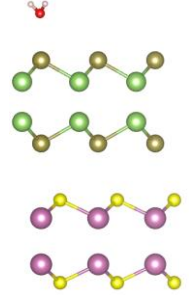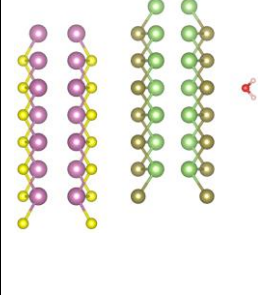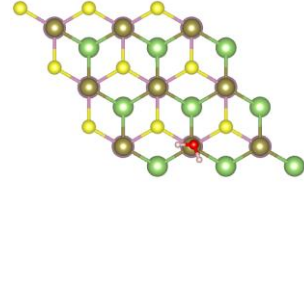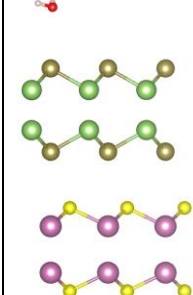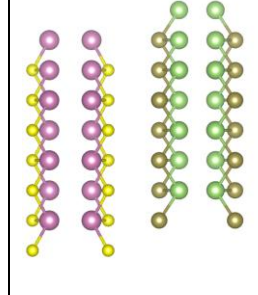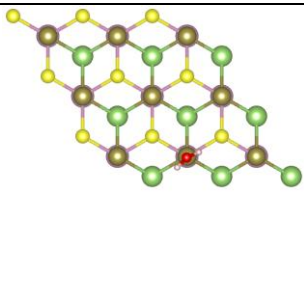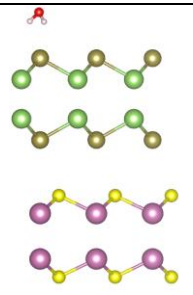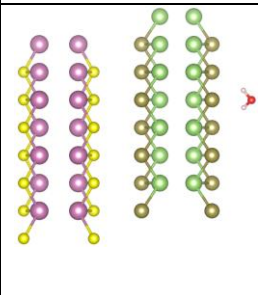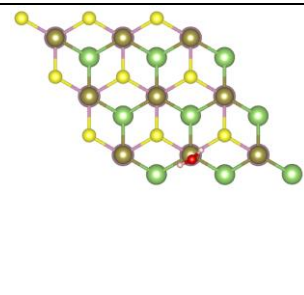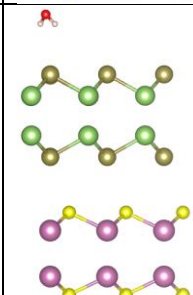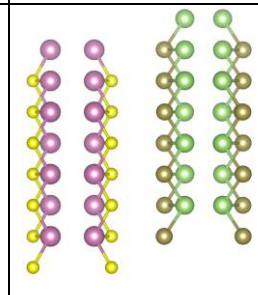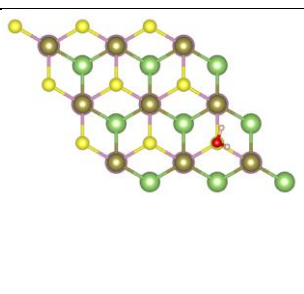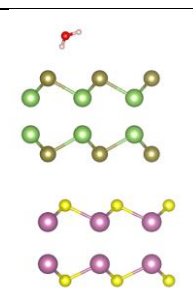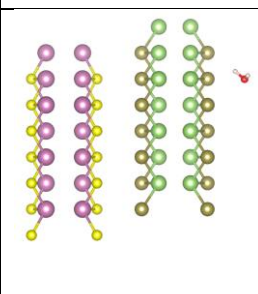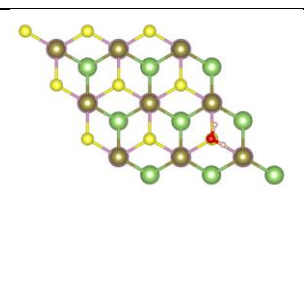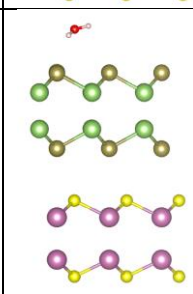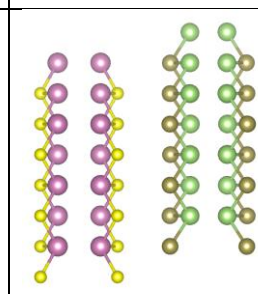
Table S6. H$_2$O adsorption on the GaTe surface.
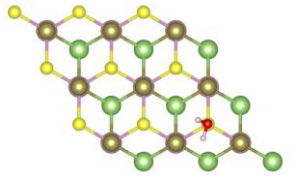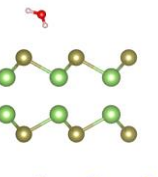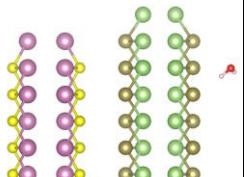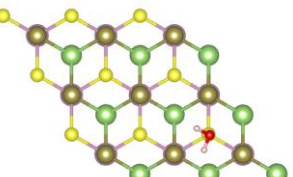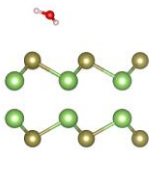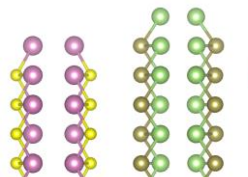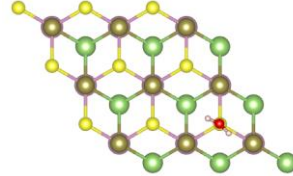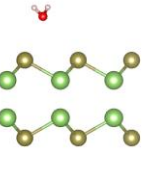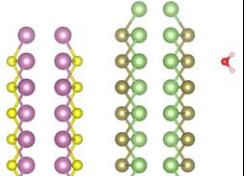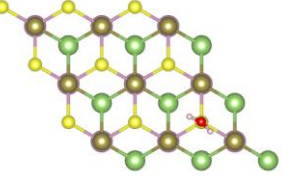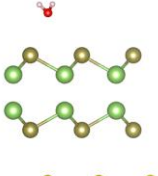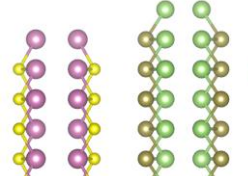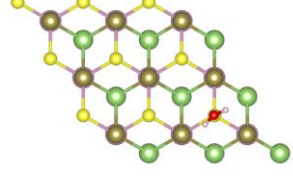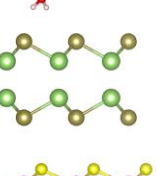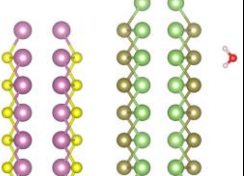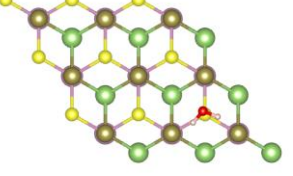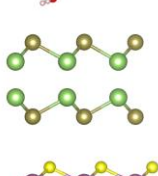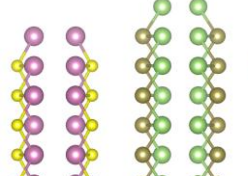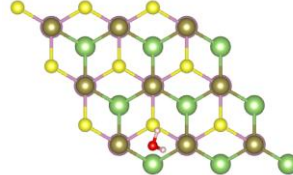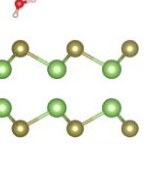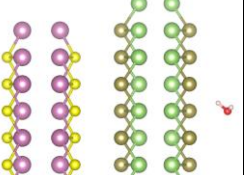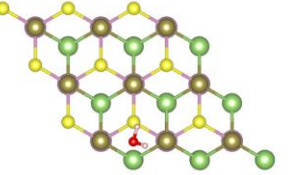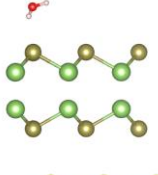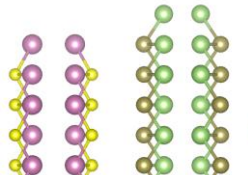
There are 6 different H$_2$O adsorption sites considered, each with 4 different rotation angles of H$_2$O. The optimized structures with the corresponding adsorption energy are presented in the following table, along with the initial configurations. The most favourable configuration is the configuration number 16 (highlighted in green) with adsorption energy of -0.152 eV.
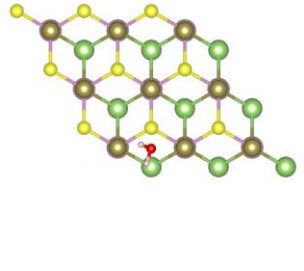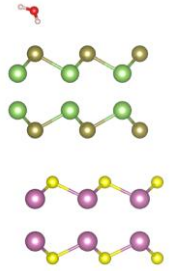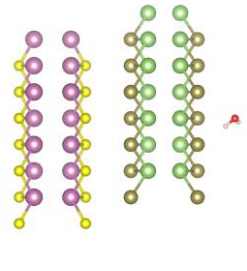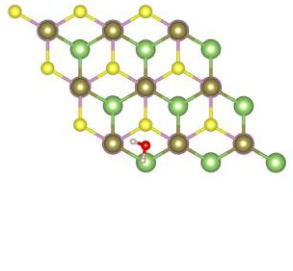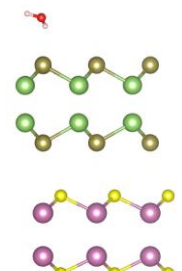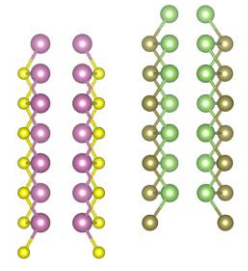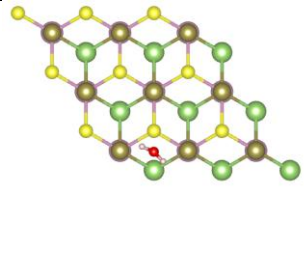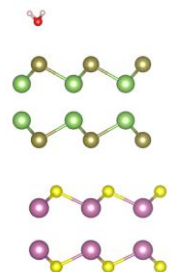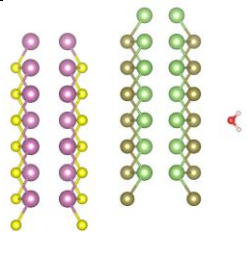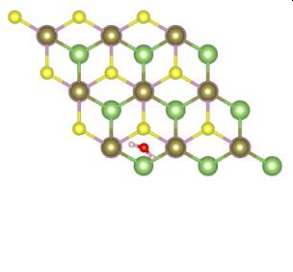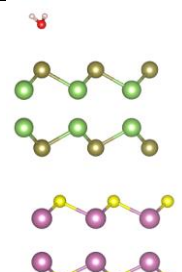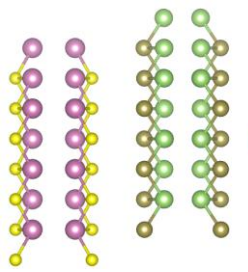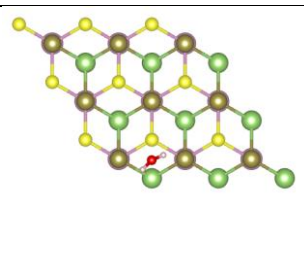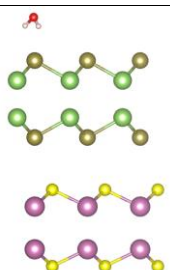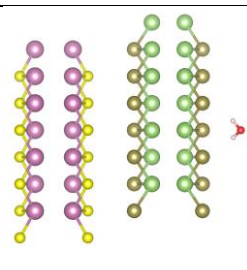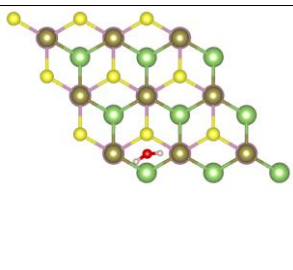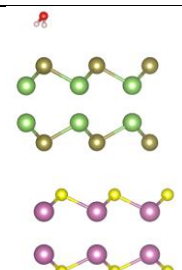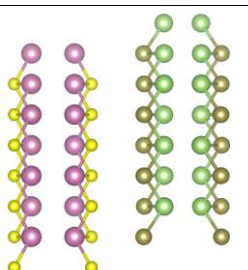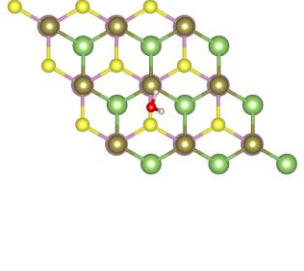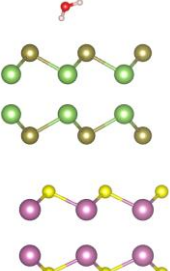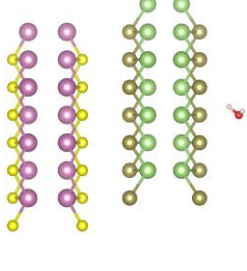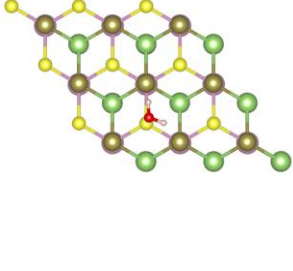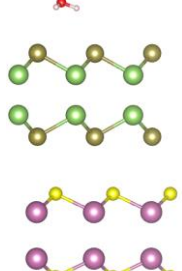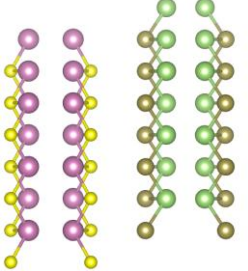
No	Initial			Optimized			E_ads (eV)
	Top	Side-1	Side-2	Top	Side-1	Side-2	
1							-0.128
2							-0.147
3							-0.118

4							-0.150
5							-0.116
6							-0.111
7							-0.095

8		-0.133
9		-0.116
10		-0.116

11						-0.063
12						-0.096
13						-0.152

14						-0.132
15						-0.121
16						-0.152
17						-0.131

18							-0.136
19							-0.112
20							-0.144
21							-0.150
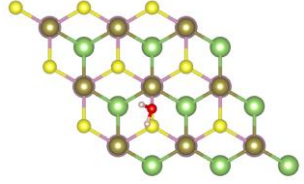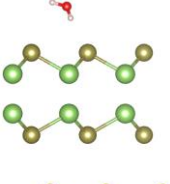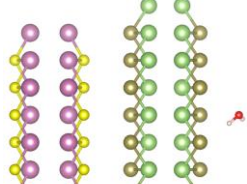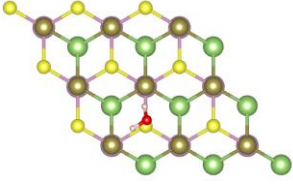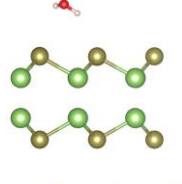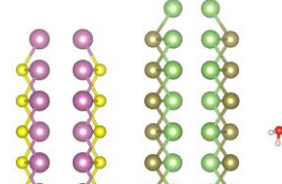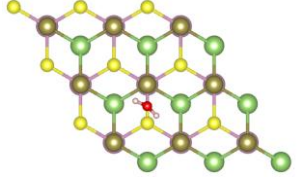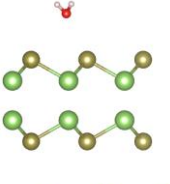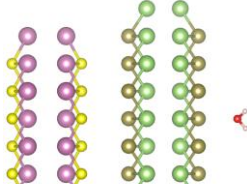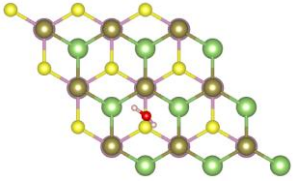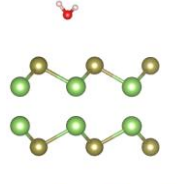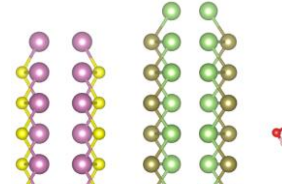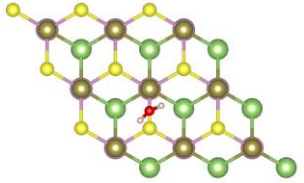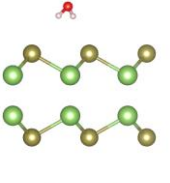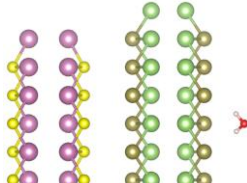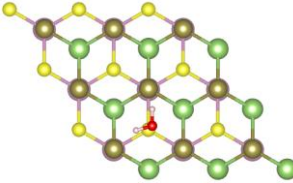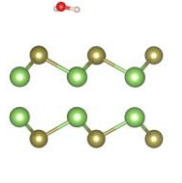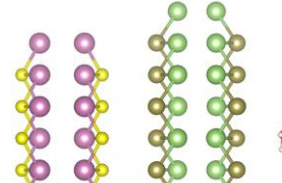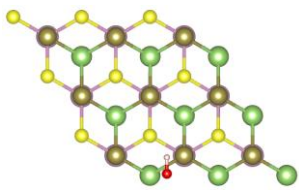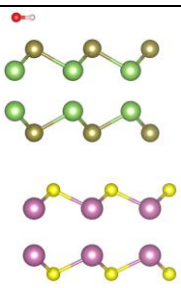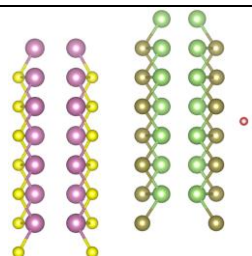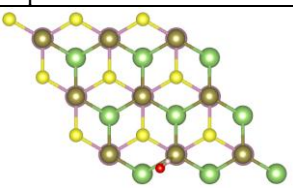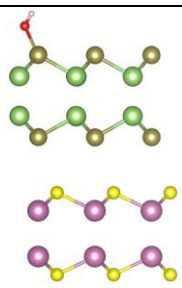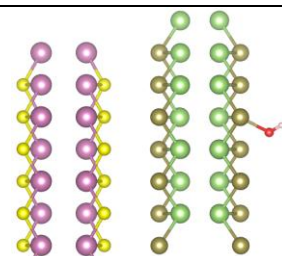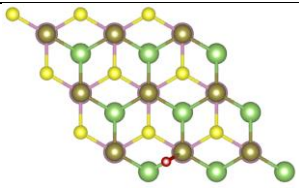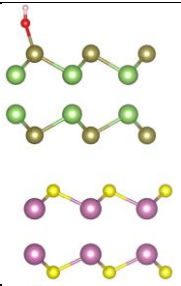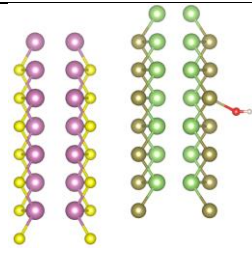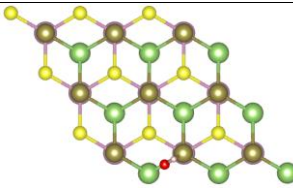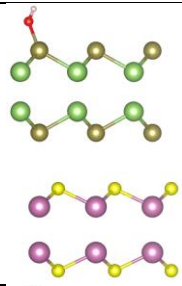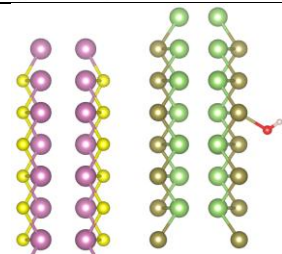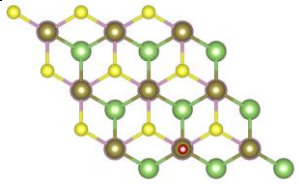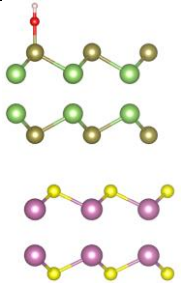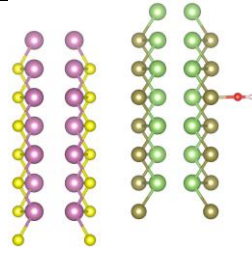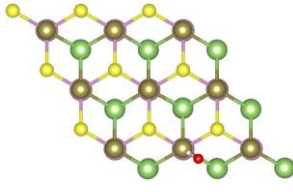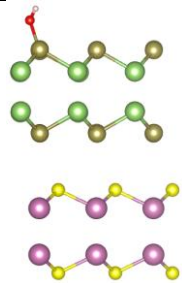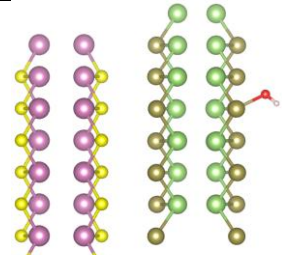
							-0.150
22							-0.150
23							-0.104
24							-0.150

Table S7. OH adsorption on the GaTe surface.

24 different configurations were studied, from which 6 stable adsorption sites were obtained. The optimized structures with the corresponding adsorption energy are presented in the following table, along with the initial configurations. Configuration number 5 (highlighted in green) is the most favourable one with adsorption energy of -1.714 eV.

No	Initial			Optimized			E_ads (eV)
	Top	Side-1	Side-2	Top	Side-1	Side-2	
1							-1.622
2							-1.622
3							-1.623

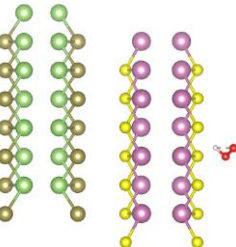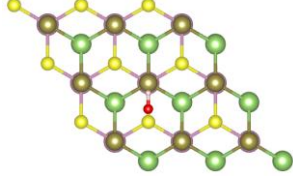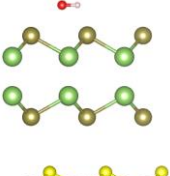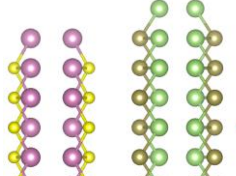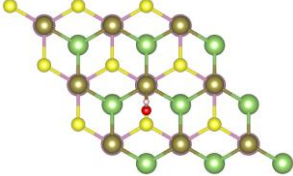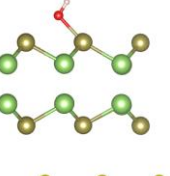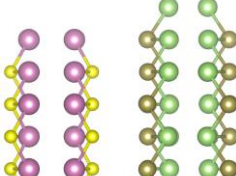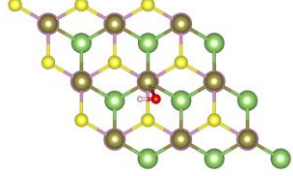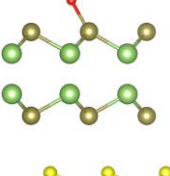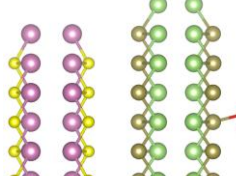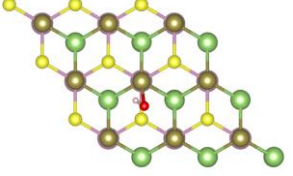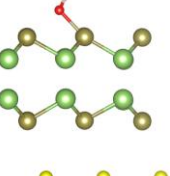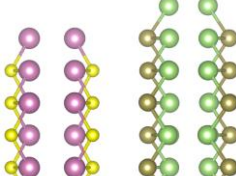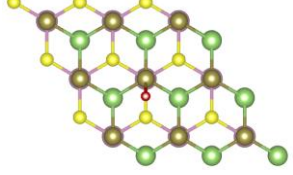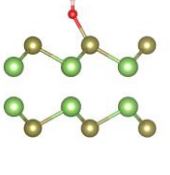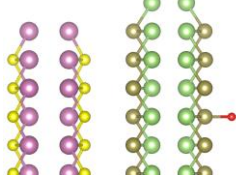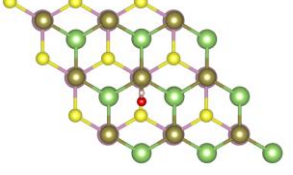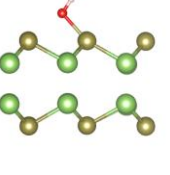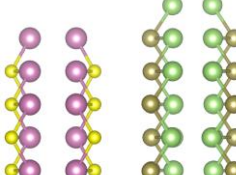|							
4							-1.707
5							-1.7136
6							-1.7135

Table S8. O adsorption on the GaTe surface.

6 different configurations were studied, from which O was stably adsorbed in 3 configurations. The optimized structures with the corresponding adsorption energy are presented in the following table, along with the initial configurations. Configuration number 3 (highlighted in green) is the most favourable one with adsorption energy of -4.325 eV. It is interesting to note that all the optimized structures imply that the only site for the adsorption of O is on the top of S, with essentially the same adsorption energy of around -4.3 eV.
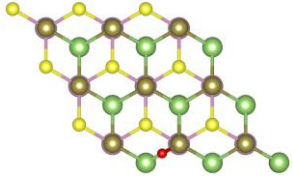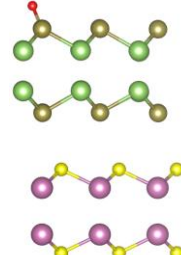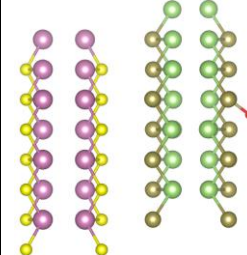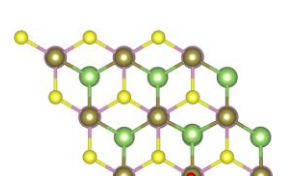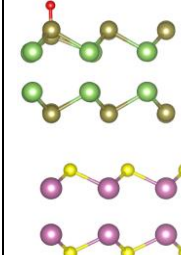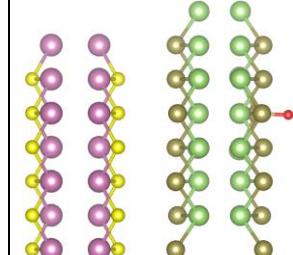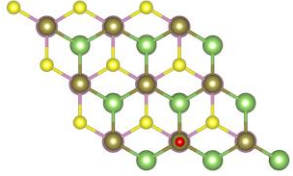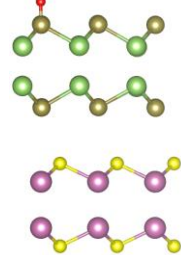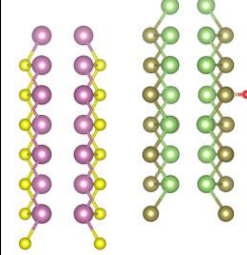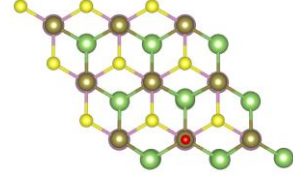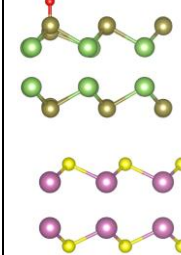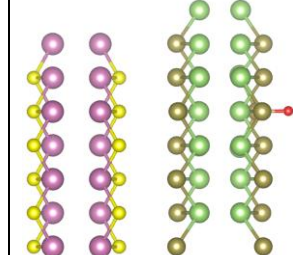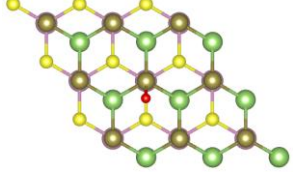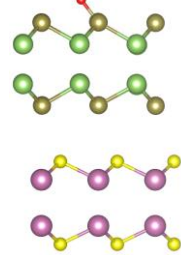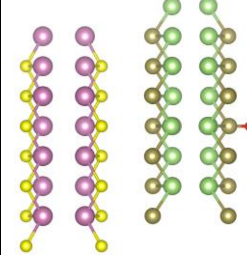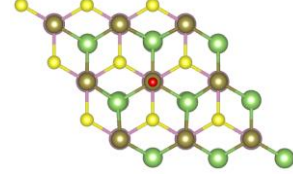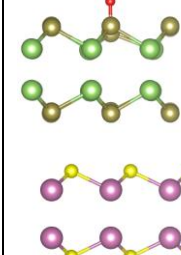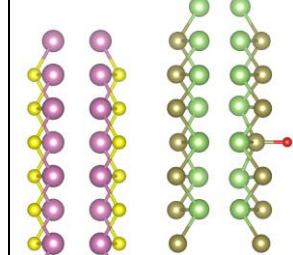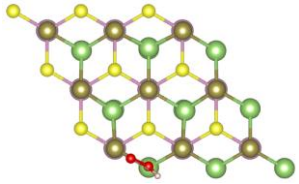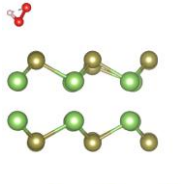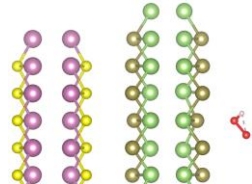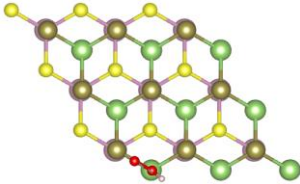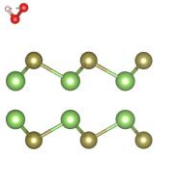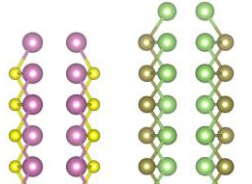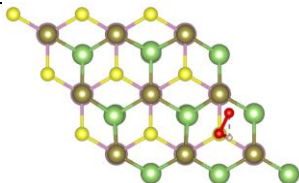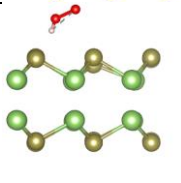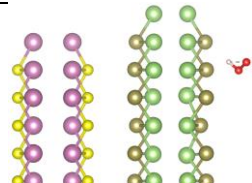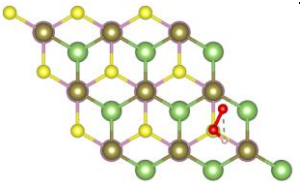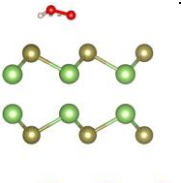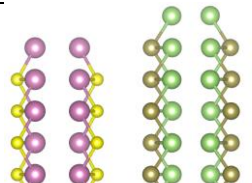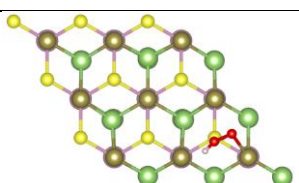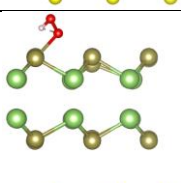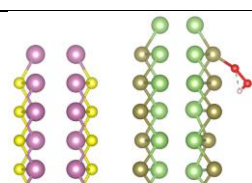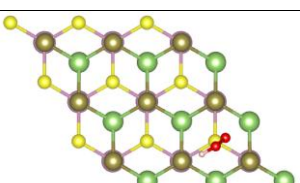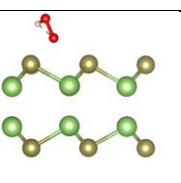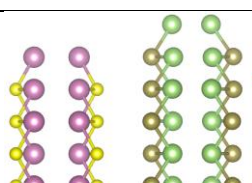
No	Initial			Optimized			E_ads (eV)
	Top	Side-1	Side-2	Top	Side-1	Side-2	
1							-4.310
2							-4.311
3							-4.325

Table S9. OOH adsorption on the GaTe surface.

24 different configurations were studied, which resulted in 4 stable configurations. The optimized structures with the corresponding adsorption energy are presented in the following table, along with the initial configurations. The configuration number 3 (highlighted in green) is the most favourable one with adsorption energy of -0.62 eV.

No	Initial			Optimized			E_ads (eV)
	Top	Side-1	Side-2	Top	Side-1	Side-2	
1							-0.24
2							-0.47
3							-0.62
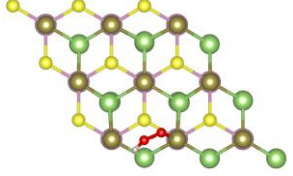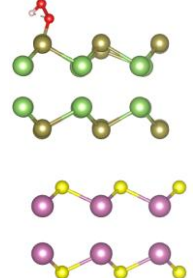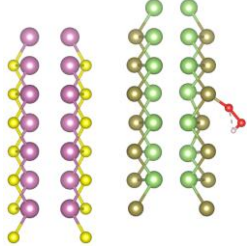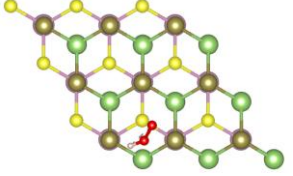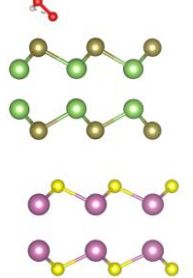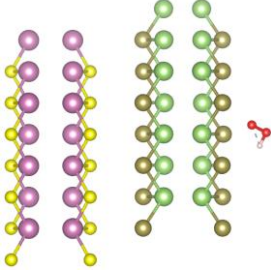
| 4 | | -0.57 |

Table S10. Data of the photogenerated electron potential (U_e), hole potential (U_h), the corresponding pH dependence of the potential ($G_{U(e)}$ and $G_{U(h)}$), and the pH effect on the Gibbs free energy (G_{pH}), used for the calculation of the Gibbs free energy difference for Z-Scheme and type-II Scheme.

Scheme	pH	$U_{e(SHE)}$ (eV)	$G_{U(e)}$ (eV)	$U_{h(SHE)}$ (eV)	$G_{U(h)}$ (eV)	G_{pH} (eV)
Z-scheme	0	0.000	0.000	0.000	0.000	0.000
	1	0.000	-0.059	0.000	0.059	0.059
	2	0.000	-0.118	0.000	0.118	0.118
	3	0.000	-0.177	0.000	0.177	0.177
	4	0.000	-0.236	0.000	0.236	0.236
	5	0.000	-0.295	0.000	0.295	0.295
	6	0.000	-0.354	0.000	0.354	0.354
	7	0.000	-0.413	0.000	0.413	0.414
	0	1.080	1.080	2.369	2.369	0.000
	1	1.021	0.962	2.428	2.487	0.059
	2	0.962	0.844	2.487	2.605	0.118
	3	0.903	0.726	2.546	2.723	0.177
	4	0.844	0.608	2.605	2.841	0.236
	5	0.785	0.490	2.664	2.959	0.295
	6	0.726	0.372	2.723	3.077	0.354
	7	0.667	0.254	2.782	3.195	0.414
Type-II	0	-	-	0.000	0.000	0.000
	1	-	-	0.000	0.059	0.059
	2	-	-	0.000	0.118	0.118
	3	-	-	0.000	0.177	0.177
	4	-	-	0.000	0.236	0.236
	5	-	-	0.000	0.295	0.295
	6	-	-	0.000	0.354	0.354
	7	-	-	0.000	0.413	0.414
	0	-	-	1.440	1.440	0.000
	1	-	-	1.499	1.558	0.059
	2	-	-	1.558	1.676	0.118
	3	-	-	1.617	1.794	0.177
	4	-	-	1.676	1.912	0.236

	5	-	-	1.735	2.030	0.295
	6	-	-	1.794	2.148	0.354
	7	-	-	1.853	2.266	0.414

Table S11. Numerical values of the relative OER free energy for the Z-Scheme and the type-II scheme.

Scheme	Step	G (eV)							
		$pH = 0$	$pH = 1$	$pH = 2$	$pH = 3$	$pH = 4$	$pH = 5$	$pH = 6$	$pH = 7$
Z-scheme		Light-off							
	H_2O (l)	0.000	0.000	0.000	0.000	0.000	0.000	0.000	0.000
	OH*	2.137	2.019	1.901	1.783	1.665	1.546	1.428	1.310
	O*	2.720	2.483	2.247	2.011	1.774	1.538	1.302	1.066
	OOH*	5.288	4.933	4.579	4.224	3.870	3.515	3.161	2.806
	O_2 (g) + *	4.756	4.280	3.807	3.335	2.862	2.389	1.917	1.444
		Light-on							
	H_2O (l)	0.000	0.000	0.000	0.000	0.000	0.000	0.000	0.000
	OH*	-0.232	-0.409	-0.586	-0.763	-0.940	-1.118	-1.295	-1.472
	O*	-2.018	-2.373	-2.727	-3.081	-3.436	-3.790	-4.144	-4.498
	OOH*	-1.819	-2.351	-2.882	-3.414	-3.945	-4.477	-5.008	-5.540
	O_2 (g) + *	-4.720	-5.429	-6.137	-6.846	-7.554	-8.263	-8.972	-9.680
Type-II		Light-off							
	H_2O (l)	0.000	0.000	0.000	0.000	0.000	0.000	0.000	0.000
	OH*	1.819	1.701	1.583	1.465	1.347	1.229	1.110	0.992
	O*	3.259	3.023	2.787	2.550	2.314	2.078	1.841	1.605
	OOH*	5.191	4.837	4.482	4.128	3.773	3.419	3.064	2.710
	O_2 (g) + *	4.895	4.481	4.008	3.536	3.063	2.591	2.118	1.645
		Light-on							
	H_2O (l)	0.000	0.000	0.000	0.000	0.000	0.000	0.000	0.000
	OH*	0.379	0.202	0.025	-0.152	-0.329	-0.506	-0.684	-0.861
	O*	0.379	0.025	-0.329	-0.684	-1.038	-1.392	-1.747	-2.101
	OOH*	0.871	0.340	-0.192	-0.723	-1.255	-1.786	-2.318	-2.849
	O_2 (g) + *	-0.806	-1.515	-2.224	-2.932	-3.641	-4.349	-5.058	-5.767

Table S12. Numerical values of the ZPE, entropy (ΔS), the total energy (E), and the temperature (T=298.15 K), for the calculation of the free energy

System	E (eV)	ZPE (eV)	$T\Delta S$ (eV)
H_2O (l)	-599.171	0.558 [2]	0.025 [3]
OH*	-194,104	0.011	0.090
O*	-194,088	0.003	0.029
OOH*	-194,659	0.036	0.093
H_2 (g)	-30.900	0.258 [4]	0.403

Table S13. The HER and OER overpotentials for Z-scheme of the InS/GaTe heterostructure for different pH values. pH = 0 and pH = 1 are not included as OER reactions are predicted to be not spontaneous for these two pH values.

pH	$\chi(H_2)(eV)$	$\chi(O_2)(eV)$
2	0.962	1.258
3	0.903	1.317
4	0.844	1.376
5	0.785	1.435
6	0.726	1.494
7	0.667	1.553
8	0.608	1.612
9	0.549	1.671
10	0.490	1.730
11	0.431	1.789
12	0.372	1.848
13	0.313	1.907
14	0.254	1.966

Table S14. Variation in the overpotential and solar to hydrogen efficiency for inaccuracy in the band gap by ±0.1 eV. The predicted efficiency is 44.8% (E_g=1.34 eV).

Band gap is inaccurate by -0.1 eV (E_g = 1.24 eV)					η_{STH} (%)
	Case 1		Case 2		
	χ (H$_2$)	χ (O$_2$)	χ (H$_2$)	χ (O$_2$)	
pH=0	0.980	1.140	1.080	1.040	48.60
pH=1	0.921	1.199	1.021	1.099	48.60
pH=2	0.862	1.258	0.962	1.158	48.60
pH=3	0.803	1.317	0.903	1.217	48.60
pH=4	0.744	1.376	0.844	1.276	48.60
pH=5	0.685	1.435	0.785	1.335	48.60
pH=6	0.626	1.494	0.726	1.394	48.60
pH=7	0.567	1.553	0.667	1.453	48.60
pH=8	0.508	1.612	0.608	1.512	48.60
pH=9	0.449	1.671	0.549	1.571	48.60
pH=10	0.390	1.730	0.490	1.630	48.60
pH=11	0.331	1.789	0.431	1.689	48.60
pH=12	0.272	1.848	0.372	1.748	48.60
pH=13	0.213	1.907	0.313	1.807	48.60
pH=14	0.154	1.966	0.254	1.866	42.55
Band gap is inaccurate by +0.1 eV (E_g = 1.44 eV)					
	Case 1		Case 2		
	χ (H$_2$)	χ (O$_2$)	χ (H$_2$)	χ (O$_2$)	
pH=0	1.180	1.140	1.080	1.240	39.85
pH=1	1.121	1.199	1.021	1.299	39.85
pH=2	1.062	1.258	0.962	1.358	39.85
pH=3	1.003	1.317	0.903	1.417	39.85
pH=4	0.944	1.376	0.844	1.476	39.85
pH=5	0.885	1.435	0.785	1.535	39.85
pH=6	0.826	1.494	0.726	1.594	39.85
pH=7	0.767	1.553	0.667	1.653	39.85

pH=8	0.708	1.612	0.608	1.712	39.85
pH=9	0.649	1.671	0.549	1.771	39.85
pH=10	0.590	1.730	0.490	1.830	39.85
pH=11	0.531	1.789	0.431	1.889	39.85
pH=12	0.472	1.848	0.372	1.948	39.85
pH=13	0.413	1.907	0.313	2.007	39.85
pH=14	0.354	1.966	0.254	2.066	39.85

Details on the effect of band deviation on water splitting efficiency:

The deviation of -0.1 eV (+0.1 eV) in the band gap can be due to the shift of the CB of InS to a lower (higher) energy region and or that of the VB of GaTe to a higher (lower) energy region. The total shift of the two cases must equal 0.1 eV. Such changes will not only change the band gap but also the HER and OER overpotentials and therefore η_{sth}. Here, it is only necessary to analyse the two extreme cases for which HER and OER overpotentials will experience the most significant change. The first case is for -0.1 eV (+0.1 eV), we shift the CB of InS by 0.1 eV to a lower (higher) energy while the VB of GaTe remains un-shifted. The second case is we shift the VB of GaTe by 0.1 eV to a higher (lower) energy while the CB of InS remains unchanged. As seen from the table, the OER and HER overpotential values for all pH are larger than 0.6 eV and 0.2 eV, respectively, except for pH = 14 (band is off by -0.1 eV) where the HER overpotential is 0.154 eV. This implies that E = Eg = 1.34 eV still applies for these cases except for pH = 14 where E = Eg + 0.2 − χ(H$_2$) = 1.39 eV (Eq. 41).

Details on the effect of overpotential on water splitting efficiency:

Even though overpotentials above the thresholds of 0.2 eV (HER) and 0.6 eV (OER) give the same η_{sth}, it is recommended to keep overpotentials as low as possible to reduce energy losses and improve overall efficiency in applications. Table S13 and S14[†] show that in general, χ(H$_2$) decreases for increasing pH while the reverse is true for χ(O$_2$). However, as χ(O$_2$) is generally higher than χ(H$_2$) for all pH, InS/GaTe is predicted to achieve better overall efficiency for low pH values (acid to neutral environment) as it would result in relatively small energy losses in real applications (due to lower overpotentials) compared to basic environment even though the theoretically predicted η_{sth} values are the same.

Table S15. Comparison between the OER Gibbs free energy and overpotential (χ) of InS/GaTe and RuO_2 and IrO_2 [5]. All quantities are in eV. The potential determining steps are in bold.

Catalyst	pH	ΔG_1	ΔG_2	ΔG_3	ΔG_4	χ
RuO_2 (110)		0.90	1.17	**2.10**	0.75	0.87
IrO_2 (110)		0.22	1.29	**2.42**	0.99	1.19
InS/GaTe	0	2.08	0.56	**2.56**	-0.47	1.14
	1	1.96	0.44	**2.45**	-0.59	1.20
	2	1.84	0.32	**2.33**	-0.71	1.26
	3	1.72	0.20	**2.21**	-0.83	1.32
	4	1.61	0.08	**2.09**	-0.95	1.38
	5	1.49	-0.03	**1.97**	-1.06	1.44
	6	1.37	-0.15	**1.86**	-1.18	1.49
	7	1.25	-0.27	**1.74**	-1.30	1.55
	8	1.13	-0.39	**1.62**	-1.42	1.61
	9	1.02	-0.51	**1.50**	-1.54	1.67
	10	0.90	-0.63	**1.38**	-1.65	1.73
	11	0.78	-0.74	**1.26**	-1.77	1.79
	12	0.66	-0.86	**1.15**	-1.89	1.85
	13	0.54	-0.98	**1.03**	-2.01	1.91
	14	0.43	-1.10	**0.91**	-2.13	1.97

References

1. Yang, G., and Gao, S-P., 2021. A method to restore the intrinsic dielectric functions of 2D materials in periodic calculations. Nanoscale, 2021,13, 17057-17067. https://doi.org/10.1039/D1NR04896A
2. Tiwari A., Honingh C., and Ensing B. Accurate calculation of zero point energy from molecular dynamics simulations of liquids and their mixtures. J. Chem. Phys. 151, 244124 (2019). https://doi.org/10.1063/1.5131145
3. Bagchi B. The entropy of water. Water in Biological and Chemical Processes From Structure and Dynamics to Function, 2013. pp. 287 - 304. Cambridge University Press. https://doi.org/10.1017/CBO9781139583947.024
4. NIST Computational Chemistry Comparison and Benchmark Database, NIST Standard Reference Database Number 101 Release 22, May 2022, Editor: Russell D. Johnson III. https://doi.org/10.18434/T47C7Z
5. Alexandra Z., and Vitaly A. ACS Catal. 2020, 10, 6, 3650–3657. https://doi.org/10.1021/acscatal.9b05544